NASA/TM—2010-216091

A Compendium of Scale Surface Microstructures: Ni(Pt)Al Coatings Oxidized at 1150 °C for 2000 1-h Cycles

James L. Smialek
Glenn Research Center, Cleveland, Ohio

Anita Garg
The University of Toledo, Toledo, Ohio

February 2010

NASA STI Program . . . in Profile

Since its founding, NASA has been dedicated to the advancement of aeronautics and space science. The NASA Scientific and Technical Information (STI) program plays a key part in helping NASA maintain this important role.

The NASA STI Program operates under the auspices of the Agency Chief Information Officer. It collects, organizes, provides for archiving, and disseminates NASA's STI. The NASA STI program provides access to the NASA Aeronautics and Space Database and its public interface, the NASA Technical Reports Server, thus providing one of the largest collections of aeronautical and space science STI in the world. Results are published in both non-NASA channels and by NASA in the NASA STI Report Series, which includes the following report types:

- TECHNICAL PUBLICATION. Reports of completed research or a major significant phase of research that present the results of NASA programs and include extensive data or theoretical analysis. Includes compilations of significant scientific and technical data and information deemed to be of continuing reference value. NASA counterpart of peer-reviewed formal professional papers but has less stringent limitations on manuscript length and extent of graphic presentations.

- TECHNICAL MEMORANDUM. Scientific and technical findings that are preliminary or of specialized interest, e.g., quick release reports, working papers, and bibliographies that contain minimal annotation. Does not contain extensive analysis.

- CONTRACTOR REPORT. Scientific and technical findings by NASA-sponsored contractors and grantees.

- CONFERENCE PUBLICATION. Collected papers from scientific and technical conferences, symposia, seminars, or other meetings sponsored or cosponsored by NASA.

- SPECIAL PUBLICATION. Scientific, technical, or historical information from NASA programs, projects, and missions, often concerned with subjects having substantial public interest.

- TECHNICAL TRANSLATION. English-language translations of foreign scientific and technical material pertinent to NASA's mission.

Specialized services also include creating custom thesauri, building customized databases, organizing and publishing research results.

For more information about the NASA STI program, see the following:

- Access the NASA STI program home page at *http://www.sti.nasa.gov*

- E-mail your question via the Internet to *help@sti.nasa.gov*

- Fax your question to the NASA STI Help Desk at 443–757–5803

- Telephone the NASA STI Help Desk at 443–757–5802

- Write to:
  NASA Center for AeroSpace Information (CASI)
  7115 Standard Drive
  Hanover, MD 21076–1320

NASA/TM—2010-216091

A Compendium of Scale Surface Microstructures: Ni(Pt)Al Coatings Oxidized at 1150 °C for 2000 1-h Cycles

James L. Smialek
Glenn Research Center, Cleveland, Ohio

Anita Garg
The University of Toledo, Toledo, Ohio

National Aeronautics and
Space Administration

Glenn Research Center
Cleveland, Ohio 44135

February 2010

Acknowledgments

The authors would like to acknowledge J.A. Nesbitt for associated microprobe work, R. Rogers and R. Mattingly for x-ray diffraction. V.K. Tolpygo is acknowledged for numerous very helpful discussions regarding characterization of alumina scales and Ni(Pt)Al coatings.

This work was sponsored by the Fundamental Aeronautics Program at the NASA Glenn Research Center.

Level of Review: This material has been technically reviewed by technical management.

Available from

NASA Center for Aerospace Information
7115 Standard Drive
Hanover, MD 21076–1320

National Technical Information Service
5285 Port Royal Road
Springfield, VA 22161

Available electronically at http://gltrs.grc.nasa.gov

A Compendium of Scale Surface Microstructures: Ni(Pt)Al Coatings Oxidized at 1150 °C for 2000 1-h Cycles

James L. Smialek
National Aeronautics and Space Administration
Glenn Research Center
Cleveland, Ohio 44135

Anita Garg
The University of Toledo
Toledo, Ohio 43606

Abstract

The surface structure of scales formed on Ni(Pt)Al coatings was characterized by SEM/EDS/BSE in plan view. Two, nominally identical, {100} samples of aluminide coated CMSX–4 single crystal were oxidized at 1150 °C for 2000 1-h cycles and were found to produce somewhat disparate behavior. One sample, with less propensity for coating grain boundary ridge deformation, presented primarily α-Al_2O_3 scale structures, with minimal weight loss and spallation. The original scale structure, still retained over most of the sample, consisted of the classic θ-α transformation-induced ridge network structure, with ~25 nm crystallographic steps and terraces indicative of surface rearrangement to low energy alumina planes. The scale grain boundary ridges were often decorated with a fine, uniform distribution of (Hf,Ti)O_2 particles. Another sample, producing steady state weight losses, exhibited much interfacial spallation and a complex assortment of different structures. Broad areas of interfacial spalling, crystallographically-faceted (Ni,Co)(Al,Cr)$_2O_4$ spinel, with an α-Al_2O_3 base scale, were the dominant features. Other regions exhibited nodular spinel grains, with fine or (Ta,Ti)-rich (rutile) particles decorating or interspersed with the spinel. While these features were consistent with a coating that presented more deformation at extruded grain boundaries, the root cause of the different behavior between the duplicate samples could not be conclusively identified.

Introduction

Platinum-modified aluminides are widely used as oxidation resistant coatings or bond coats for thermal barrier coatings (TBC) on single crystal superalloy turbine blades. They are noted for forming protective α-Al_2O_3 scales with greater longevity and adherence compared to similarly processed aluminides without Pt and generally operate for thousands of hours, with peak metal temperatures around 1050 °C. They are produced by electroplating ~5 μm of Pt, diffusion heat treating, and aluminizing by CVD or pack. While processing details have largely remained in the realm of the commercial coating vendors, coating characterization and performance have been studied intensively in recent years. Important phenomena typically addressed are: (1) Growth of web-like θ-α Al_2O_3 transformation scale structures; (2) The tendency for alumina scales to wrinkle and bond coats to rumple, leading to TBC interface instability (Refs. 1 and 2); (3) Improved scale adhesion for substrates with high Hf and low S (Ref. 3) the tendency for reduced S segregation and void formation due to Pt (Refs. 3 and 4); (4) Reduced moisture-induced scale spallation sensitivity due to Pt (Refs. 5 and 6); and (5) Formation of an ordered $L1_o$ tetragonal martensite phase after Al depletion by interdiffusion with the substrate (Refs. 7 and 8).

In the course of these studies, various morphological features, such as the web-like alumina morphology (topic 1, above), are customarily revealed by SEM characterization. These are generally directed for coatings well within their protective lifetimes and do not necessarily exhibit features indicative of imminent failure. However, the present study addresses scale microstructure after 2000 1-h

cycles at 1150 °C for Ni(Pt)Al coatings on single crystal CMSX–4. Accordingly, features indicating various degrees of coating breakdown by interdiffusion, rumpling, spallation, and oxidation are revealed.

It is a companion study to a previous work that focused on weight change and moisture-induced delayed spallation for the same samples (Ref. 9). In that study, nominally replicate samples showed either:

1. Good cyclic oxidation for the entire test, with good scale adhesion (+0.36 mg/cm^2), decreased coating grain boundary rumpling, and high moisture resistance; or
2. More substantial rumpling, increased spallation (–3.51 mg/cm^2), and moisture-induced delayed spallation, measurable up to 1 day after cooldown.

Indeed, these two samples represent somewhat the limits of behavior for a spectrum of cyclic oxidation results obtained for 6 replicate samples in the same test, from 100 to 2000 cycles. The following contributes to a more comprehensive catalogue of the myriad structures that develop with continued high-temperature cycling. It is a complement to various microstructures presented in the broader literature for cyclic oxidation of Ni(Pt)Al coatings, as highlighted in the discussion later.

Experimental

Coupons of superalloy (CMSX–4) were machined from 0.38- by 2.54- by 15.2-cm (1/8- by 1- by 6-in.) cast single crystal slabs (PCC) with {100} faces and <100> growth direction. They were coated with a commercial Ni(Pt)Al aluminide coating (MDC-150L, Howmet Corporation, Whitehall, Michigan). The charge material came from the same master ingot and the machined oxidation samples were coated in the same batch. (They were provided by Dr. Kang Lee, Rolls-Royce Corporation, Indianapolis, Indiana, as part of a Metals Affordability Initiative (MAI) study, sponsored by WPAFB, Donna Ballard, Program Manager.) Briefly, the Pt was electrodeposited to a thickness of about 5^+ μm and aluminized in a low activity CVD process.

The samples were approximately 3.2-mm by 1.27- by 2.54-cm, with a 2.3-mm diam. hanger hole at one end. The samples had a surface area approximately 9.1 cm^2 and weighed approximately 9 g each. They were ultrasonically cleaned in detergent, rinsed in water then ethanol, and dried. Samples were cyclically oxidized at 1150 °C, suspended by Pt hang wires, in a vertical, six alumina tube furnace, using a 60 min. heating cycle and a 20 min. cooling cycle for 2000 cycles. Cycling was accomplished by a pneumatic cylinder-actuated assembly, controlled by electronic timers and counters. The furnace control temperature was constant, remaining within 1 to 2 °C throughout the test. Hot zone variations ranged up to 5 °C, depending on the individual tube. During each cooling cycle, the samples were retracted into a baffled chamber above the furnace, providing some barrier to direct thermal drafts from the hot tubes below. However, the environment was still relatively warm and dry, maintaining ~100 to 130 °C while the ambient room conditions were only 20 to 25 °C.

With continued testing, it was observed that the samples exhibiting more weight change (growth and spallation) also presented some delayed spallation, occurring up to a day after the initial cooldown. This phenomenon became apparent after 750 cycles, and weight measurements were made over time at ambient to track any delayed spallation. Exposure to additional moisture (1-h water immersion) was performed at the end of the 2000 h test. These details of these results were presented in the previous publication (Ref. 9).

Optical macrographs were obtained over the course of the test to document overall spallation patterns, while SEM/EDS was performed at the end of the test using a Hitachi 4700 FEG/SEM to reveal detailed scale morphology and chemistry. The samples were carbon coated for most EDS and BSE imaging studies. Generally, 15 kV operating voltages were used for BSE elemental differentiation and complete EDS spectra. Corresponding SE images were obtained at 15, 6 and 1 kV. Afterwards one half of the coupon face was gold/palladium coated for higher resolution imaging at 6 kV.

Results

As-Coated

A polished cross-section of an as-coated sample had been characterized by electron microprobe WDS scans (Ref. 10). The as-coated thickness, measured from the surface to the included alumina particles (from the initial grit blast surface prep), was 37±1 μm. Composition varied somewhat across the layer, but was nominally 50Ni – 8Co – 8Pt – 35Al – 4Cr – 0.5Ta (at. %). (This compares to previous work reporting 45Ni – 3.5Co – 6Pt – 44Al – 1.5Cr or 46.5Ni – 4.5Co – 5.5Pt – 39.6Al – 3.6Cr – 0.2Ta – 0.1W for this coating on René N5 (Refs. 1 and 7)). Some of the TCP phases lie within the coating, above the diffusion zone + TCP region. The latter was an additional 30 μm thick.

The as-coated surface morphology of sister samples contained grain boundary ridges (Ref. 9), typical of CVD Ni(Pt)Al coatings (Refs. 4 and 5). The EDS response of the overall coating, grain interiors, and grain boundaries was generally similar, showing basically uniform amounts of Ni, Pt, Al with a small amount of Cr, Fe, and Co (Ref. 9). However, no analyses were performed on the actual oxidation coupons before testing.

Weight Change

The overall total 1150 °C, 2000 h weight change behavior (due to normal cycling and any delayed spallation) was reported in Part I (Ref. 9). The oxidation response of one sample (1150–4) increased to a maximum of +0.5 mg/cm^2 at 1350 h and displayed a very small spallation rate afterwards, ending at +0.4 mg/cm^2. A nominally duplicate sample (1150–2) indicated a fairly typical increase to a maximum of 0.8 mg/cm^2 at 460 h, followed by an approximately linear loss rate to –3.3 mg/cm^2. (Four other duplicates, tested for times between 100 to 1000 h, as part of a broader study, showed a similar range of responses). Thus, higher growth rates and higher spallation rates are noted for sample 2 compared to sample 4 and appear to bound the range of behavior for these samples.

Sample 1150–4 SEM

The final surface morphology is exemplified in Figure 1(a) for sample 1150–4 that gained less overall weight and remained positive through the end of the test, while exhibiting smoother surface texture and less spalling to bare metal. More details are revealed in the sequence of increasing magnification, Figures 1(b) to (e). Numerous cracked ridges can be seen in Figure 1(b), as well as the undulating nature of the surface. It is now quite wrinkled, with the primary eruptions at what appear to be the grain boundaries of the Ni(Pt)Al coating. These eruptions have roughly a 100 μm spacing and are well documented in the literature. Figure 1(c), a higher magnification image of the area marked C in Figure 1(b), reveals numerous cracks and some spalled areas. Figure 1(d) of area D highlights a number of these cracked (arrows) and damaged coating ridge areas and also shows a variety of web-like scale ridge structures. These areas are believed to represent the originally formed scale, where no spalling or regrowth has taken place. Finally, a ruptured peak, cracking, and freshly exposed bare metal are presented in Figure 1e, with imprints from the oxide grains ranging from about 0.5 to 2 μm.

In this sample, only a few isolated areas of spalling to bare metal are observed by BSE imaging, Figure 2(a). EDS of the exposed oxide grain boundary imprint area, marked B in Figure 2(a) and shown in detail in Figure 2(b), reveals Ni, Al, W, Pt, Ti, Cr, and Co (Fig. 2(c)), all components of the Ni(Pt)Al diffusion coating found by EPMA. (Note: The W peak can include left and right shoulders of overlapping Ta and Re peaks, respectively).

Other broad distinctions were oxide scale regions of fine nodular and coarse plate-like grains, Regions I and II in Figure 3. The region marked b in Figure 3(a) is shown in detail in Figure 3(b). Region II is seen to be a dense, uniform array of ~0.2 μm nodules growing on top of a fine ridged network at the increasing magnification of Figures 3(b) and (c). In Figure 3(d), which is a magnified view of Frame D in

Figure 3(b), it appears that the overall nodular region is depressed from surrounding areas and may represent a spalled area that has regrown a scale thinner than adjacent unspalled areas. In these adjacent areas, with exposed cross-section features, the individual grains are sometimes highlighted by a ridge of oxide, indicating some outward growth of alumina by grain boundary diffusion of aluminum. Another example of an edge exposed by prior spallation and regrowth is shown in Figure 4.

The larger grain structure present in Region I of Figure 3(a) and similar areas represents the majority of the surface. It is believed that these areas exhibit unspalled regions of the original scale. They are characterized by variations of the oxide ridge network, Figure 5, circumscribing thinner plate-like grains, typically displayed by isothermal or unspalled scales formed on β-phase NiAl intermetallic alloys. In backscatter, Figure 6, it is seen that the ridges are peppered with a very fine, ≤0.1 μm, nearly spherical, bright second phase. EDS analyses at 15 kV for the bright particle marked H in Figure 7, shows that Hf was present in addition to Al and O. Whereas, the underlying ridge material and adjacent plate, A1 and A2, respectively, exhibit no Hf peak and essentially the same EDS spectra, Figure 7. (Since the analyzed area is likely to be on the order of 1 μm, the Hf spectra also include a large amount of surrounding and supporting alumina material).

An additional size effect was observed for bright particles in Figure 8. Here a range of particle sizes is apparent, and the associated 15 kV EDS spectra follow a trend of increasing Ti content with particle size, N, M, L, Figure 9. However all the particles maintain a relatively constant Hf peak, indicating a mixed Hf-Ti oxide. These are compared to the Hf-Ti absent spectra for nonparticle regions, O.

Finally the interior plates of the ridge network are examined. Here Au-Pd coated areas and 6 kV were more helpful for attaining higher resolution than the carbon coating and the 15 kV used for EDS and BSE. An example is shown in Figure 10(a), which at higher magnification, Figure 10(b), exhibits arrays of crystallographic facets in these otherwise featureless platelets. Another example is given in Figure 11(a), where now even some of the ridge nodules exhibit distinct crystallographic faceting. At higher magnification, Figure 11(b), the facets can be seen as a quite complex assemblage of fine steps and terraces. Assuming an approximate facet orientation of 45° to the plane of the figure, one series of equally spaced steps and terraces was estimated to have a characteristic dimension of about 24 nm and will be discussed later.

Sample 1150–2 SEM

This sample surface became much more complex than 1150–4 because of early and repeated spallation events scattered across the surface, as shown in Figure 10 of Reference 9. Many of the representative complex features are contained in the region of Figure 12, as marked by four superimposed frames to be examined in detail in the BSE survey below. The most apparent feature in this backscatter image is the bright exposed bare-metal region, frame I, shown in more detail in Figure 13(a). In comparison to Figure 2 for 1150–4, the EDS spectrum of the metal now reveals lower Al and Pt, but more substantial peaks for W, Cr and Co. A case can be made that the lower Al peak is due to faster oxidation kinetics and more spallation observed on this sample, 1150–2. It can be argued that the surface phase in Figure 2 is γ'-Ni_3Al, whereas that in Figure 13(a) is γ-Ni, with a higher solubility for Cr. There are also numerous entrained, fractured scale particles, primarily alumina, which were relatively pure except for some small Ni-rich inclusions inside the pegs, Figure 13(b).

The region of frame II, expanded in Figure 14(a), exhibits a complex mosaic of backscatter intensities, implying multiple scale structures. (By comparison, the BSE structure for sample 1150–4 at the same magnification appears featureless, except for the spalled area, Fig. 2(a) or except for the fine Hf(Ti)-rich particles seen at much higher magnification, Figs. 6 to 8). The multiple features of a representative central area, II A, are examined in greater detail in Figure 14(b). The lighter scale, II A.1, is shown in Figure 15(a) to consist of arrays of faceted, triangular chevron scales, with an EDS spectra indicative of $NiAl_2O_4$. The darker Region, II A.2, of Figure 14(b) is shown to have primarily an Al_2O_3 base in Figure 15(b). The mixed scale structure, II A.3, from the right side of Figure 14(b), is shown in Figure 15(c) to have a dark base (C), with lighter 1 μm blocky crystals (A) and bright smaller 0.2 μm

particles (B,D) appearing on top. The corresponding EDS spectra indicate that these are, respectively, Al_2O_3, $NiAl_2O_4$ (with some Co and Cr), and Ta, Ti-rich oxides.

More BSE surveys, Figure 16, were obtained for Region III of Figure 12. Some familiar arrangements are seen in the upper right frame III A. Here again a dark Al_2O_3 base exists, Figure 17(a) and (b), surrounded by a grey granular scale with a dispersion of small bright particles on top.

Frame III B of Figure 16 is expanded in Figure 18. Here BSE revealed a large ~50 to 100 μm cluster of crystallographically-aligned features, frame III B.1, shown in detail in Figure 18(b). The corresponding EDS spectra was indicative of $NiAl_2O_4$. In this case, concave, pitted, or notched features were observed. The structure was often triangular or chevron, similar to those in Figure 15(b). The details are resolved more clearly for images obtained on gold-coated regions at 6 kV, with representative examples presented in Figures 19(a), (b), and (c).

In contrast, Region III C is seen to be a uniform mixture of two types of convex grains, imaged in BSE as duplex atomic weight features, Figure 20. EDS, however, revealed these to be another manifestation of $NiAl_2O_4$ grains and Ta, Ti-rich particles, III C.1a, in Figure 20(c). But here the white Ti, Ta particles (W) are approximately in the same 1 μm size range as the grey spinel grains (G), with the excited volume now contributing to much higher Ta, Ti relative peak heights. Referring back to Figure 16, it is seen that this duplex structure represents a significant area fraction of the scale.

Finally, the structures in frame IV of Figure 12 were obtained at 1 kV for a gold-coated area and are shown in Figure 21. They are presented as an SEI montage composed of 10 micrographs, numbered right to left, first shown as two detailed split strips in Figure 21(b). At higher magnification, image IV–1, Figure 22, shows the faceted concave cups or imprints of convex oxide grain surfaces left in the bare metal after scale spallation. Figure 23(a), midway across the top strip, shows another broad ~ 20 μm arrangement of highly aligned crystallographic features (from the mosaic images IV–3,4). Figure 23(b) shows image IV–7 having two 5 to 10 μm portions of facets, aligned along the inset parallelograms. Finally, Figure 23(c) presents numerous individual submicron grains which are themselves highly faceted, but not necessarily aligned with their neighbors. Based on the BSE/EDS studies above, the structures of Figure 23 appear to be the individual $NiAl_2O_4$ grains, with perhaps some Ta,Ti-rich particles.

Scale Phases

XRD for sample 1150–4 at 2000 h revealed only α-Al_2O_3 for this more resistant sample type, Figure 24. No patterns were obtained to account for the fine (Hf,Ti)-rich oxide particles. For the sample 1150–2 exhibiting more spallation, α-Al_2O_3 plus $NiAl_2O_4$ spinel (a_o = 8.05 Å) were observed as the major scale phases, after 2000 h, Figure 24. A weak pattern was observed for a rutile structure (*R*), presumably from the (Ta,Ti))O_2 oxide particles observed by SEM/BSE. Only γ/γ′ FCC metal phases were observed for both 2000 h samples, although NiAl $L1_o$ martensite had been found for other samples stopped after 100 and 1000 h.

Overview

Based on the myriad of structures documented above, simplified schematic cross-sections of the scales were constructed, as shown in Figures 25 and 26, respectively, for the protective, adherent scale on 1150–4 and the spalled and degraded scale on 1150–2. The adherent scale on 1150–2 is entirely alumina, with ~5 μm platelets (thermal faceting is too fine to represent on this scale). At each platelet boundary a grouping of fine 1 μm grains compose an oxide ridge, Figure 25(b). At these ridges, dispersed 0.2 μm (Hf,Ti)O_2 precipitates decorated the surface, with Ti content increasing with particle size. In areas near coating grain boundaries, where wrinkling and spallation were the most prevalent, a regrown α-Al_2O_3 scale is shown without much of the distinctive ridge structure apparent. Instead, numerous, uniformly distributed surface grains appear, whose size is on the same order-of-magnitude as the underlying 1 μm α-Al_2O_3 grains.

The less protective scale on 1150–2 exhibits a wider diversity of structures, Figure 26. Now we see prevalent spalling to the coating metal surface, Figure 26(a). For the scale, there are wide expanses of crystallographically faceted spinel, punctuated by more limited regions of primarily α-Al_2O_3, appearing more as isolated islands rather than broad expanses, Figure 26(b). Other areas exhibit combinations of an α-Al_2O_3 base structure, nearly fully covered with 1μm spinel grains, comingled with 1 μm or decorated with fine 0.2 $(Ta,Ti)O_2$ particles.

Discussion

The features described above are summarized in Table 1. Some of them have been seen in one form or another previously. An attempt to catalogue the surface structures reported in recent studies on Ni(Pt)Al is also given, arranged in approximate chronological order.

Sample 1150–4

Web-Like Grain Boundaries

As we review the structures found on the flatter, more adherent sample 1150–4, it is recalled that Ni(Pt)Al grain boundary ridges are widely observed (Refs. 1, 3 to 5, and 9). Also, the scale formed was primarily α-Al_2O_3. It contained the characteristic polycrystalline, web-like patterns of transformation ridges that delineate the transformation cell boundaries and radial cracks of the scale.

Grain Boundary Particles

The 0.2 μm $(Hf,Ti)O_2$ particles decorating the grain boundaries are quite reminiscent of similar fine particles found atop alumina grain boundary regions for oxidized NiAl+HfO_2 (Ref. 11). Ultimately they are a vestige of the dynamic segregation phenomenon occurring as reactive, but insoluble, elements are incorporated into growing alumina films, driven by the oxygen potential gradient. (See the comprehensive review and new imaging in (Ref. 11)). Hf is a well known beneficial additive to β-NiAl oxidation, producing reduced growth rates from reduced grain boundary diffusion and increased scale adhesion from intensified sulfur (and possibly carbon) gettering (Ref. 12). It may therefore be surmised that these precipitates imply that some improved performance has been bestowed on the coating from Hf diffusing from the substrate. The correlation of Ti with larger particles is an indication of doping "overload," meaning that the Ti getting into the scale will be contributing to enhanced scale growth and less protective behavior. It is well known that excessive TiO_2 growth can eventually lead to alumina failures; however the exact process by which this is occurs is not well established.

Fine Alumina Grains

Equiaxed α-Al_2O_3 grains appearing at the web-like boundaries are indicative of an outward growth component (Ref. 1) that apparently proceeds concurrently with nucleation. The process can be viewed as a progressive widening of this textured or roughened boundary feature, until the inner regions of the monocrystalline pancake grains exhibit a totally recrystallized surface (Ref. 13). However a different history must be evoked for broad, uniform, nodular, fine grain areas. Here it is suggested that spalling occurred sometime before, allowing Cr and other elements diffused from the substrate to influence the re-oxidation process. For example, it is known that Cr can favor direct nucleation of α-Al_2O_3 on NiAl, thus precluding the large grains resulting from the θ–α transformation. (Ref. 24).

Spalled Regions

Despite the excellent adhesion exhibited by this sample, coating grain boundary extrusion progressed and caused buckling of the overlying scale, eventually resulting in local spallation. Here the scale grain imprints were revealed, but *without* voids, in agreement with previous work (Ref. 4).

TABLE 1.—SUMMARY COMPARISON OF RECENT AND CURRENT SEM MICROSTRUCTURAL DETAILS OF OXIDIZED Ni(Pt)Al COATINGS, IN APPROXIMATE CHRONOLOGICAL ORDER

Study	Year	Coating	Substrate	Temp. (°C)	Time (h)	Cycles	Scale phases major (minor)	Features
Tolpygo, Clarke	2000	NiPtAl L.A. CVD	René N5	1200	1, 50	1	α-Al_2O_3	β-NiAl grain boundary ridges α-Al_2O_3 grain boundary ridges; web network, flat valleys
Tolpygo	2002	NiPtAl	René N5	1150	500	500	α-Al_2O_3	α-Al_2O_3 grain boundary ridges; web network coarsening ~10 nm steps/terraces in platelets
Haynes, et al.	2002	NiPtAl L.A. CVD	René N5	1150 1150	1000 100	1000 1	α-Al_2O_3	β-NiAl grain boundary ridges, scale fracture/spallation at NiAl boundaries; α-Al_2O_3 grain boundary ridges; web network, flat valleys Reduced growth rate due to Hf Increased adhesion due to Pt and Hf
Maris-Sida, et al.	2003	NiPtAl L.A. CVD	René N5	1100 1100 1100 1100	364 753 140 896	525 1004 187 1194	α-Al_2O_3 {$NiAl_2O_4$ outer scale}	α-Al_2O_3 grain boundary ridges Center of radial transformation cracks, especially with moisture. More spallation in moisture tests
Li, et al.	2003	NiPdAl H.A. Pack	IN 738	1100	200	8	α-Al_2O_3 {$NiAl_2O_4$, $NiCr_2O_4$, TiO_2}	
Spitsberg, More	2006	NiPtAl	René N5	>1050	1-3	1	α-Al_2O_3	Exclusive α-Al_2O_3 scale at TBC failure 5 μm thick
Pint, et al.	2006	NiPtAl L.A. CVD	René 142 René N5	1100	200	200		More spallation in moisture tests
Vialas, Monceau	2006	NiPtAl H.A. Pack	CMSX–4	1050	1800	6	α-Al_2O_3 {$(Al,Cr)(Ta,Ti)O_4$}	100 to 200 nm inner scale particles
Hou, Tolpygo	2007	NiPtAl L.A. CVD	CMSX–4	1150	333	2000	α-Al_2O_3	β-NiAl grain boundary ridges α-Al_2O_3 grain boundary ridges Ridge cracking, no interface voids
Tawancy, et al.	2007	NiPtAl H.A. Pack	CMSX–4	1150	94	4	α-Al_2O_3 {Ta, Ti oxide}	1 μm Ta, Ti rich particles at scale-metal interface
Bouchaud, et al.	2008	NiAl H.A.CVD	DS ~ CMSX–4	1100	144	6	α-Al_2O_3 {$NiAl_2O_4$}	Dimpled α-Al_2O_3 grains
Smialek, Garg (this study)	2010	NiPtAl L.A. CVD	CMSX–4 (4)	1150	2000	2000	α-Al_2O_3 {$(Hf,Ti)O_2$}	Prior β-NiAl grain boundary ridges α-Al_2O_3 grain boundary ridges 25 nm thermal facets Ridge cracking, no interface voids 0.2 μm $(Hf,Ti)O_2$ g.b. particles Regrown equiaxed α-Al_2O_3 nodules
Smialek, Garg (this study)	2010	NiPtAl L.A. CVD	CMSX–4 (2)	1150	2000	2000	α-Al_2O_3 $(Ni,Co)(Al,Cr)_2O_4$, $(Ti,Ta)O_2$	Numerous spallation areas Broad 20 μm regions of faceted spinel or Ta, Ti rich surface crystals over an α-Al_2O_3 base structure

L.A. = low activity
H.A. = high activity

Steps and Terraces

The fine steps and terraces appear to be a vestige of low energy, low indice (hkil) planes. Similar high resolution features, spaced as finely as 10 nm, have been presented by Tolpygo (Ref. 13) for essentially the same coating oxidized at 1150 °C for 500 1-h cycles. He has suggested that these structures represent a reconstruction of α-Al_2O_3 surfaces to a low energy configuration according to low surface energy, low Miller indice planes.

The following summarizes various surface science studies of thermal faceting observed on bulk alumina. Such phenomena have been thoroughly documented in TEM studies of bulk α-Al_2O_3 annealed in air at 1200 to 1400 °C (Ref. 14). They identified $\{11\bar{2}0\}$ and $\{10\bar{1}0\}$ steps on (0001) α-Al_2O_3 surfaces; $(1\bar{1}02)$, $(\bar{1}102)$, and (0001) steps on $(11\bar{2}0)$ surfaces, $(1\bar{1}02)$ and $(10\bar{1}4)$ steps on $(\bar{1}012)$ surfaces, and (0001) and $\{01\bar{1}2\}$ inclined steps on the less stable $(10\bar{1}0)$ surfaces. Furthermore, the development of steps was traced by AFM studies of (0001) surfaces (Ref. 15). Initially c/6 high steps form, as predicted by the 6 different low energy configurations that may be produced by equivalent Al-Al termination layers within a unit cell. These coarsen with annealing time and temperature to form the typical step and terrace structure for (0001) α-Al_2O_3, with step height increasing from c/6 (0.217 nm) after annealing 1 hour at 1000 °C in air to primarily *c*/1 (1.30 nm) after 1 hour at 1400 °C (Ref. 16). In the case of $(10\bar{1}0)$ surfaces, inclined steps are found that produce the so-called 'hill and valley' (sawtooth) structure (Ref. 17). Recall that the finest step and terrace dimension estimated for the alumina scales (grown at 1150 °C for 2000 h) in the present study was about 24 nm, (or 10 nm for Tolpygo), i.e., about 18 times larger (or 8 times, respectively) than the basic unit cell height observed on the bulk samples.

Ni(Pt)Al Martensite

Ni(Pt)Al martensite has been clearly identified in prior studies (Refs. 7, 8, and 18). The β′-NiAl $L1_o$ face centered tetragonal martensite phase has been shown to possess lattice parameters of a = 3.78 Å and c = 3.28 Å for a coating that has been oxidized for 100 h at 1150 °C, thus reducing the aluminum content from 40 to 32 at.% (Ref. 7). Similarly, a coating that was cycled to within 28 percent of its 1150 °C cyclic life produced this β′ phase with a = 3.85 Å and c = 3.27 Å. Here we have found β′-NiAl $L1_o$ martensite for duplicate samples tested at 100 and 1000 cycles, but it does not persist out to 2000 cycles.

Sample 1150–2

Some features displayed by this more degraded sample were hinted at in prior reports, Table 1. The outer layer of spinels was somewhat prefigured by Maris-Sida (Ref. 8) (1100 °C, 364 to 896 h). However it was only found after exposure to high moisture-content environments and accounted for a mode of accelerated degradation. Otherwise, only the centers of transformation induced spoke-like cracks exhibited a limited region of spinel. These features correspond with the higher degradation rates observed for sample 1150–2 as compared to the low spinel content found on 1150–4. Spinels and rutile were also reported by Li et al. (Ref. 19) for NiPdAl after 200 h at 1100 °C and spinel was reported by Bouchard (Ref. 20) for NiAl after 144 h at 1100 °C. Vialas and Monceau (Ref. 21) reported very fine $(Al,Cr)(Ta,Ti)O_4$ rutile particles in the midsection of scales formed on NiPtAl at 1050 °C, and Tawancy et al. (Ref. 22) reported fine (Ta,Ti)-rich oxide particles for NiPtAl after 144 h at 1150 °C, but now at the scale-metal interface. In overview, there is only some correspondence between features observed on this sample with those reported in the literature, due in part to the premature NiPtAl ridge deformation here, the extensive 2000 h cyclic exposure at 1150 °C, and the repeated spallation/regrowth associated with both.

The vast preponderance of the mixed oxide scale features found here, overlying any alumina that might exist as a base layer, probably represents an intermediate but steady-state stage before total oxidative and coating failure. As such, it is probably not a morphology commonly captured for detailed study. The process by which these varied structures may arise can only be speculated at this point. Clearly

the greater rate of spallation to bare metal accelerated aluminum depletion and encouraged non-alumina phases to form on this sample at some point. Whether these mixed oxides formed first and simply reside on top of the subsequent inner healing alumina layer or whether they are actively growing layers is a matter for discussion. On one hand, a substantial amount of nonprotective oxides would be required before healing takes place. On the other hand, a substantial amount of cation diffusion through a relatively intact alumina layer would be necessary. Both routes would be special cases associated with borderline alumina formation on a depleted coating.

Summary and Concluding Remarks

Multiple samples of a commercial low-activity CVD Ni(Pt)Al coated CMSX–4 single crystal were oxidized at 1150 °C for 2000 1-h cycles. A range of spalling behavior was exhibited, correlating with initial coating grain boundary ridges and wrinkling. The present SEM/EDS/BSE microstructural studies, conducted in plan view and backed up by XRD scans of the surface, corroborate these differences.

One sample, with less propensity for coating grain boundary ridge deformation, presented primarily α-Al_2O_3 scale structures and minimal weight loss from spallation. Eventually ridge deformation became evident, but maintained exceptional scale adhesion. Relatively few areas of interfacial spalling were noted, and these revealed the characteristic imprints of oxide grains. The EDS spectra were indicative of interdiffused bond coatings showing Ni, Al, Pt, W, Cr, Co, Ti, Ta, and Mo peaks. Interdiffused coatings first corresponded to β'-martensite at earlier test times, then γ/γ'-Ni/Ni_3Al at 2000 h. Apparent regrowth over previously spalled regions exhibited a finer, more nodular-scale grain structure, while the original scale structure, still retained over most of the sample, presented the classic θ-α transformation-induced ridge network structure. The interior flat plate, monocrystal regions, circumscribed by ridges, presented dense terraces of ultrafine 25 nm crystallographic steps, indicative of surface rearrangement to low energy alumina planes. The actual ridges evolved into a more granular polycrystalline structure. These, in turn, were decorated with a fine, uniform distribution of Hf-enriched particles, presumably beneficial HfO_2. Other similar particles exhibited a range of sizes and an increase in the Ti/Hf ratio proportional to its size, probably as an $(Hf,Ti)O_2$ solid solution.

Another sample presented steady-state weight losses beginning at ~500 h. Accordingly, the scale microstructure was quite complex, showing an assortment of at least four characteristic regions with different histories (i.e., multiple spallation events and scale regrowths, possibly occurring after various times and corresponding levels of Al depletion). Many regions of fresh interfacial spalling reveal the typical oxide grain imprints and the same characteristic compositional EDS spectra mentioned above, but now with a more extensively Al-depleted surface. Broad surface areas of distinctive, crystallographically-faceted and oriented chevron structures exhibited EDS spectra indicative of $(Ni,Co)(Al,Cr)_2O_4$ spinel. Other areas exhibited a multilayered arrangement with Al_2O_3 at the base, faceted spinel grains dispersed on top of this, with fine Ta, Ti-rich (presumably rutile) particles decorating the spinel grains. Finally, large regions were observed having a dense distribution of faceted spinel grains, interdispersed with the Ta, Ti-rich particles, but now in the same size range as the spinel grains. Little evidence of the distinctive oxide ridge network, characteristic of the original transformed α-Al_2O_3 scale microstructure, was observed on this sample.

The two samples represent some limits of behavior for this type of coating. At one end, very adherent behavior is associated with the initially smoother coating grain surface structure and a lower oxidation rate. Even after wrinkling became prominent after 2000 1-h cycles, the scale is remarkably adherent. It showed substantial areas having the original α-Al_2O_3 scale structure, as supported by the nearly flat weight change curve. Only Ti was apparent as any compositional deterioration to this scale, modifying the HfO_2 grain boundary particles. At the other end of performance, wrinkling and spallation commenced earlier, and no areas were found that would suggest the original scale structure. Spallation depleted the aluminum in the coating and resulted in regrowth of a degraded scale, with features indicating that $(Ni,Co)(Al,Cr)_2O_4$ spinel was the major surface scale. Al_2O_3 was primarily observed as a sublayer. The only compositional clue that may explain this degree of variation between the two samples was the

observation of beneficial Hf in the scale on the more adherent sample and detrimental Ti in the scale on the less protective sample. However, these features may have been correlations or results of oxidative behavior rather than causative factors.

In any event, both samples provide features that serve as performance indicators. For the better sample, the well-developed oxide ridge structure implies the original scale structure and minimal prior spallation. The thinner scales regrown after a spallation event did not produce such distinctive ridge networks and were finer grain due to Cr diffusion to the interface, resulting in early nucleation/ stabilization of a fine-grained α-Al_2O_3 phase. The ridge network was all but absent on the sample exhibiting more spallation and degradation. Large crystallographically-aligned facetted spinel scales and equiaxed, distinctive Ta,Ti rich oxides grains now became the dominant features in BSE imaging, with alumina existing primarily as an underlying base oxide.

Sample 1150–4 SEM

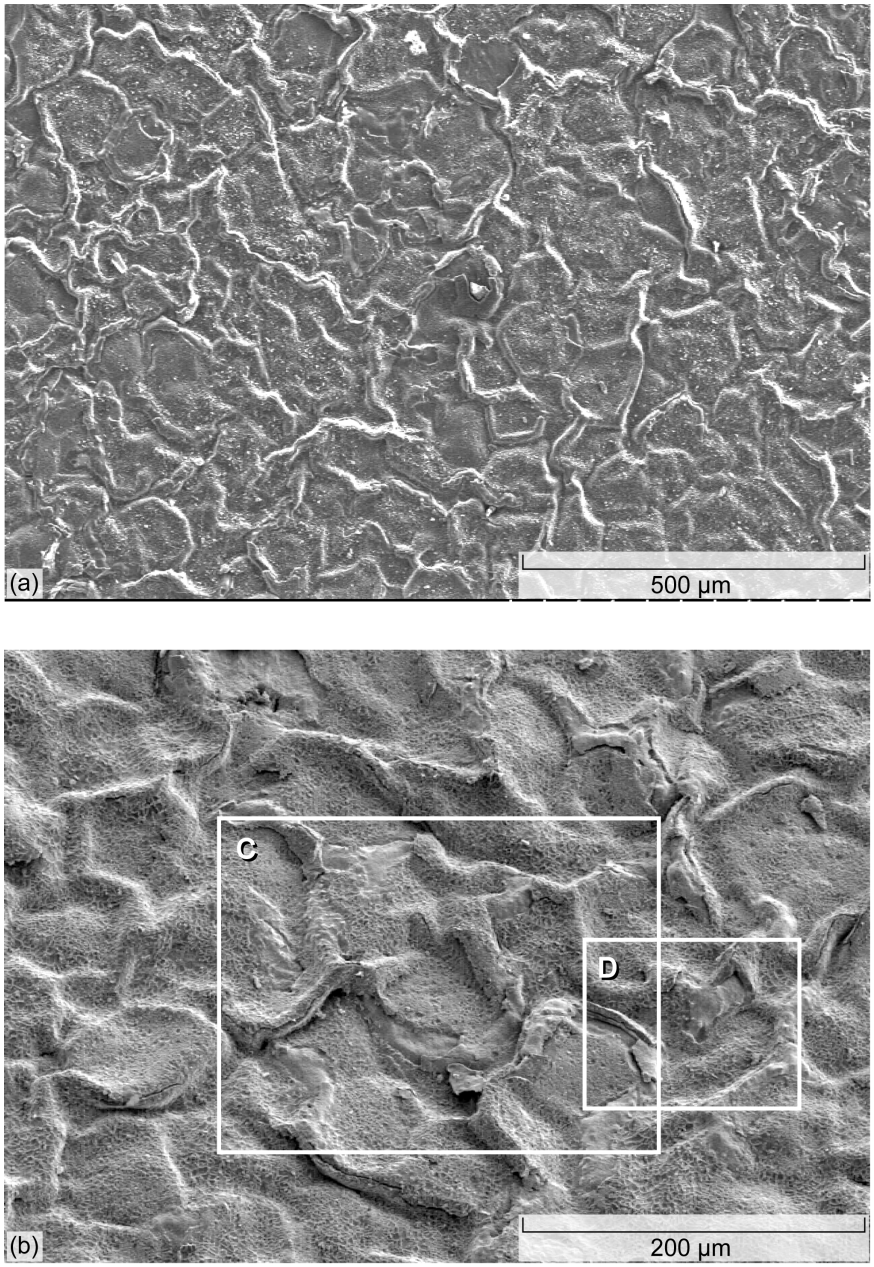

Figure 1.—Surface features of Ni(Pt)Al-coated CMSX–4, sample 1150–4, after 2000 1-hr oxidation cycles at 1150 °C. (a) Low-magnification overview showing distinct grain boundary rumpling covering entire surface, (15 kV). (b) Higher magnification reveals an assortment of ridges, cracking, and spalling, (6 kV). (c) Detail of frame C marked in (b), highlighting (arrows) a few examples of these features. (d) Detail of frame D marked in (b), (6 kV). (e) Detail of frame E marked in (d) showing multiple cracks (arrows) and detached tent of scale above a coating grain boundary ridge. Oxide grain imprints in exposed metal surface, (6 kV).

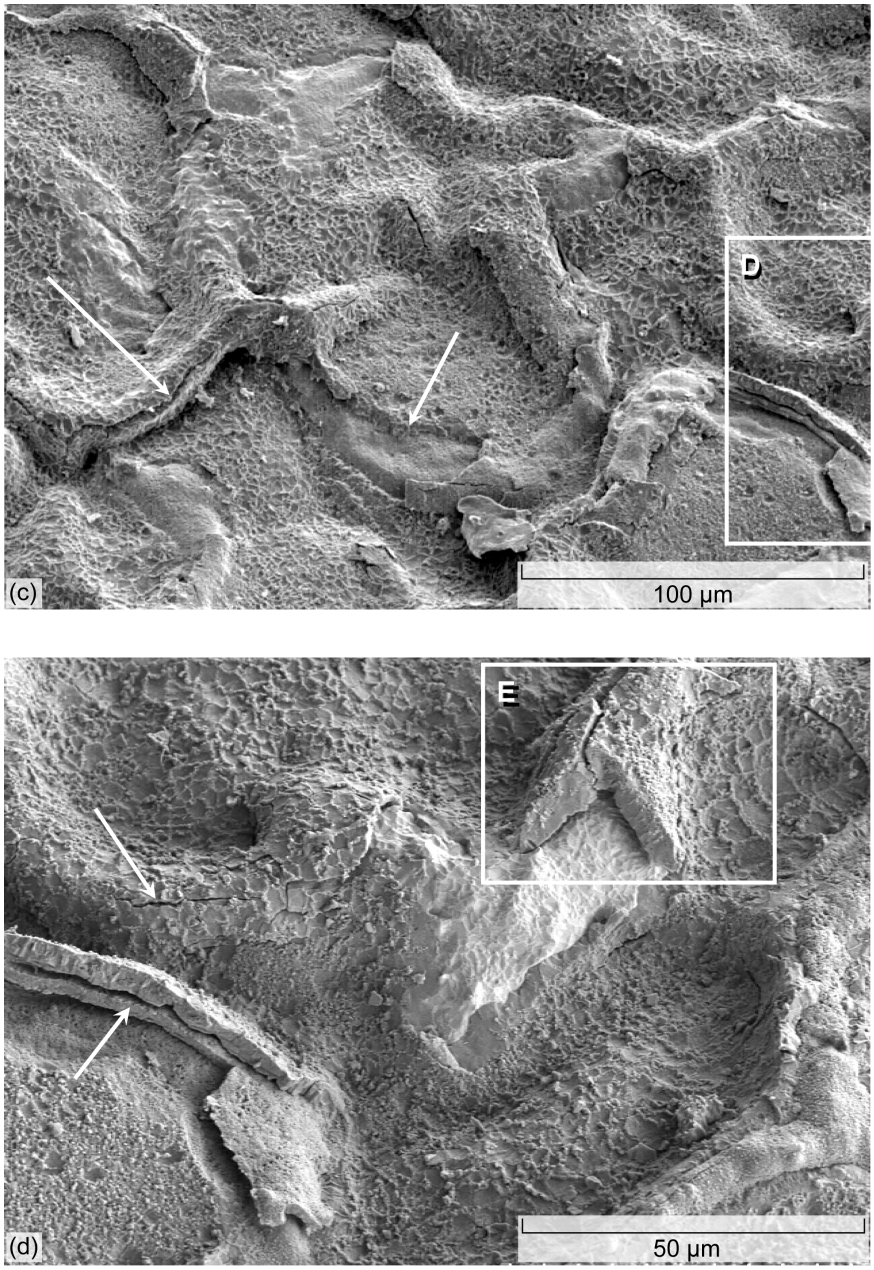

Figure 1.—Continued. (c) Detail of frame C marked in (b), highlighting (arrows) a few examples of these features. (d) Detail of frame D marked in (b), (6 kV).

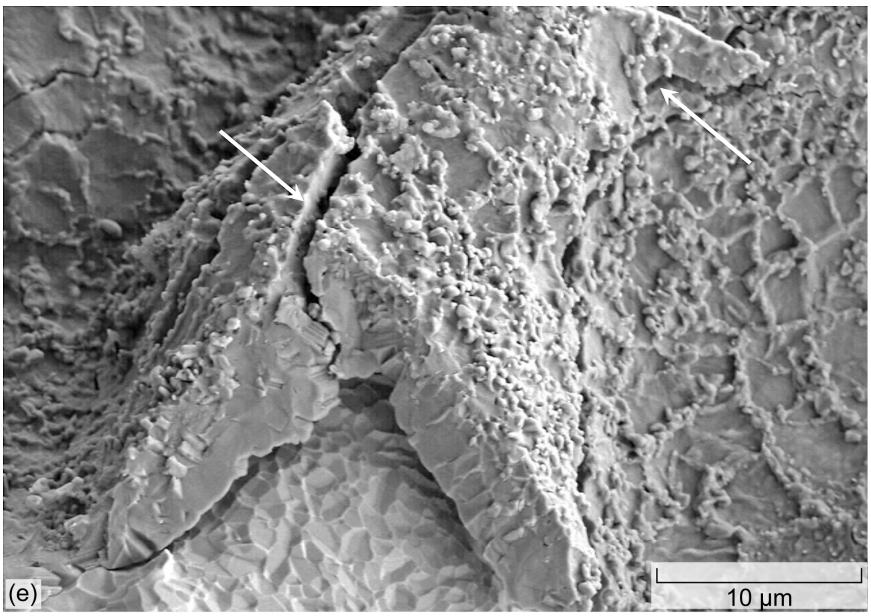

Figure 1.—Concluded. (e) Detail of frame E marked in (d) showing multiple cracks (arrows) and detached tent of scale above a coating grain boundary ridge. Oxide grain imprints in exposed metal surface, (6 kV).

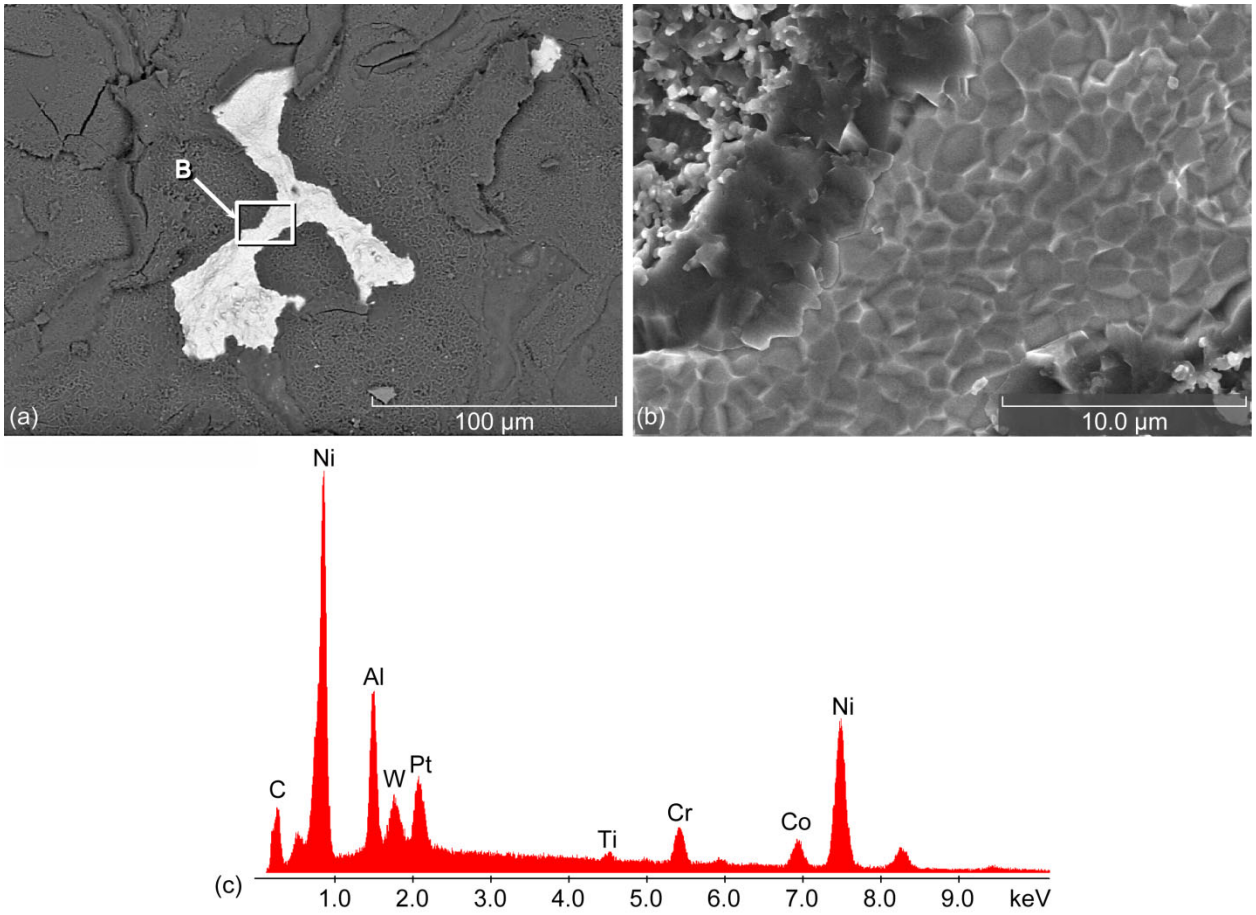

Figure 2.—Spalled region in sample 1150–4, (15 kV). (a) BSE overview showing limited extent of spalling. (b) SE details of frame marked in (a) showing imprints in bare metal. (c) EDS spectra of bare metal showing considerable Ni, Pt, Al coating and C, W, Ti, Cr, Co substrate elements.

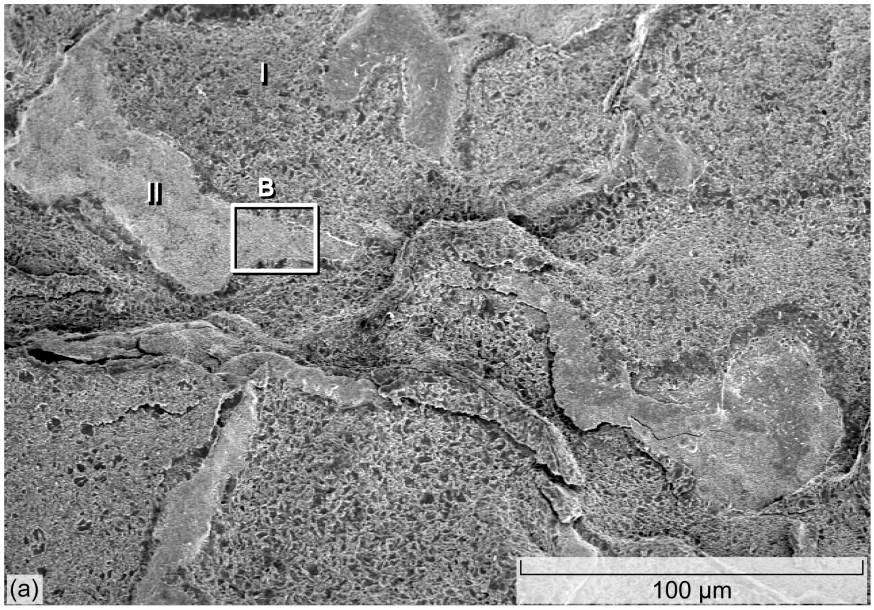

Region II

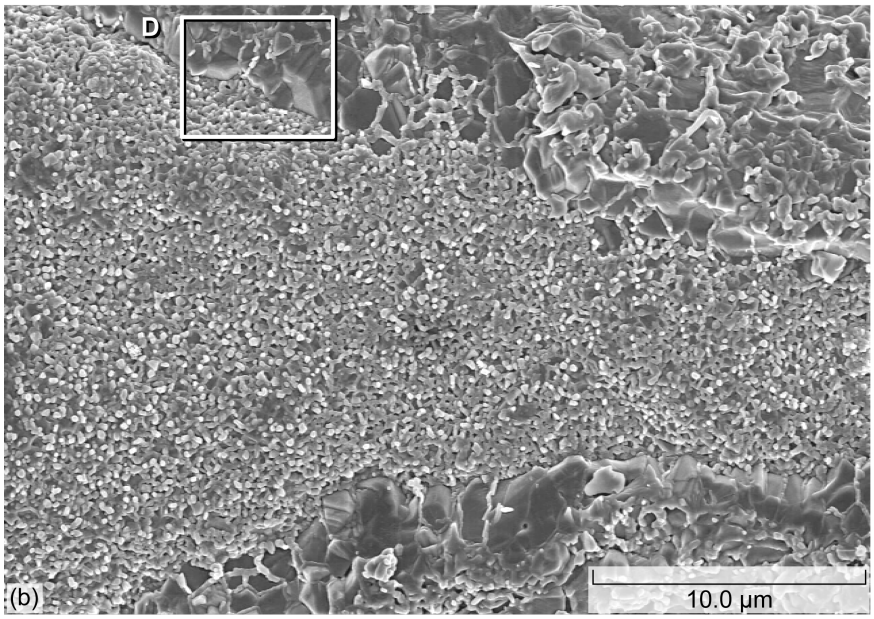

Figure 3.—Duplex scale structure for sample 1150–4, (6 kV). (a) Web structure in type I Al_2O_3 oxide and fine nodular grains in type II. (b) Detail of frame B marked in 3(a) showing mainly fine nodular grains. (c) Nodular and fine web-like features (arrows) of Region II. (d) Boundary of types I and II oxide regions marked as frame D in (b). The exposed fracture interface of type I scale reveals faceted grains and grain boundary growth ribbons (arrows).

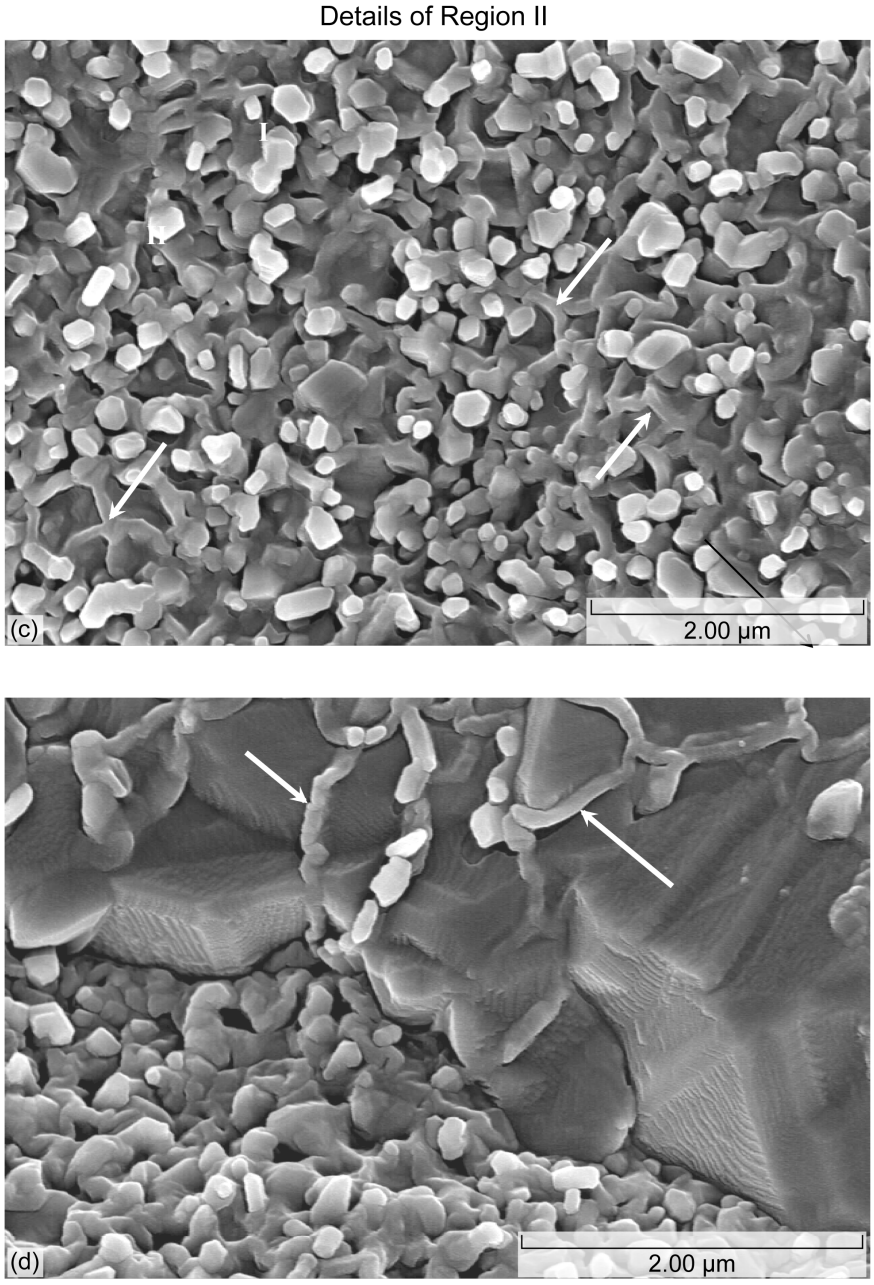

Figure 3.—Concluded. (c) Nodular and fine web-like features (arrows) of Region II. (d) Boundary of types I and II oxide regions marked as frame D in (b). The exposed fracture interface of type I scale reveals faceted grains and grain boundary growth ribbons (arrows).

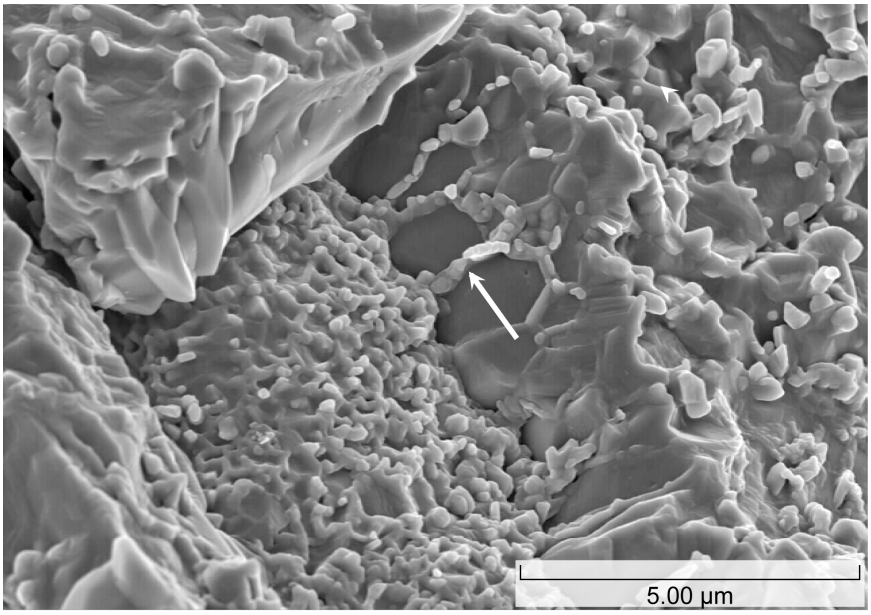

Figure 4.—Another example of the types I and II interface of sample 1150–4, revealing exposed type I grains decorated by grain boundary ribbon growth (arrow), (6 kV).

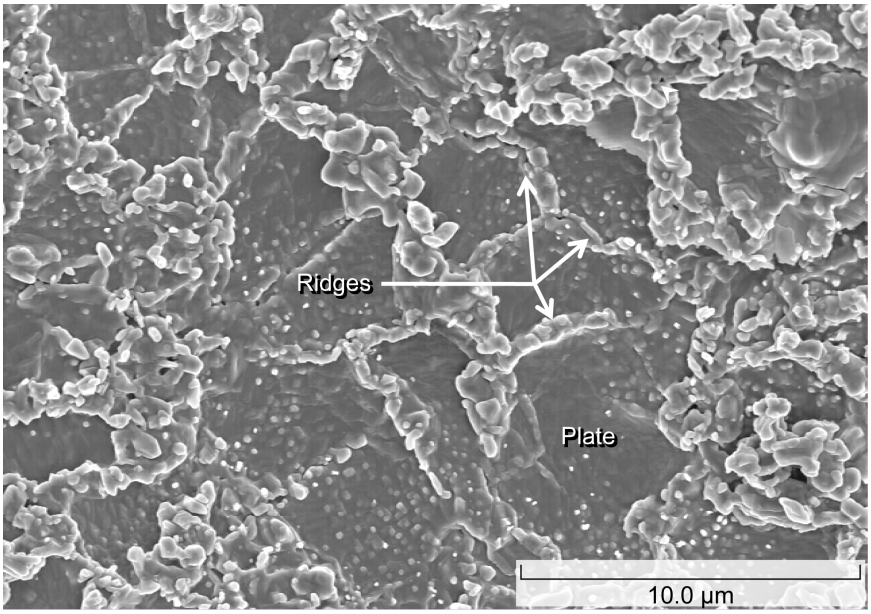

Figure 5.—Typical type I web-like oxide ridge network, showing nodulated grain boundary ridges and relatively flat central grain areas (plate), (6 kV).

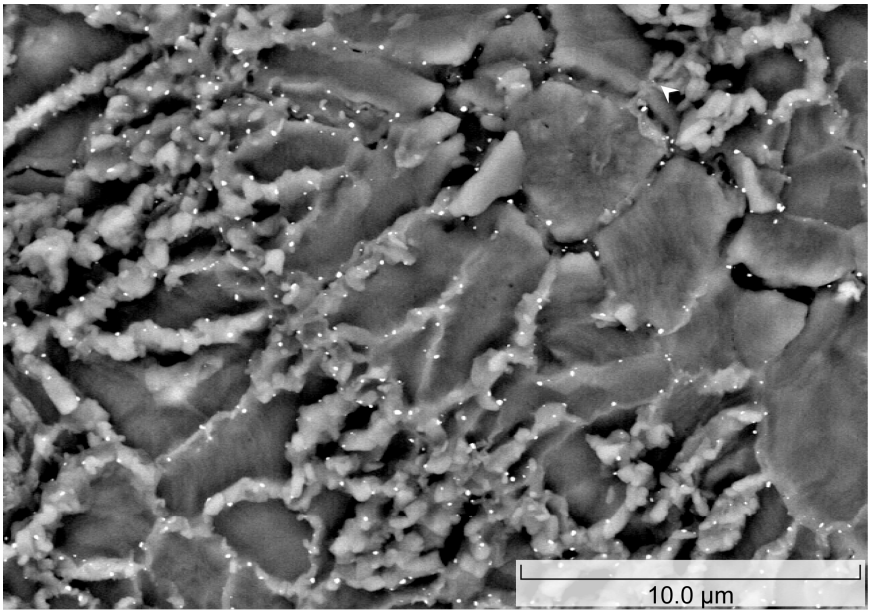

Figure 6.—BSE image (new area) of type I web-like structure showing dispersion of fine bright particles over just the grain boundary regions, (15 kV).

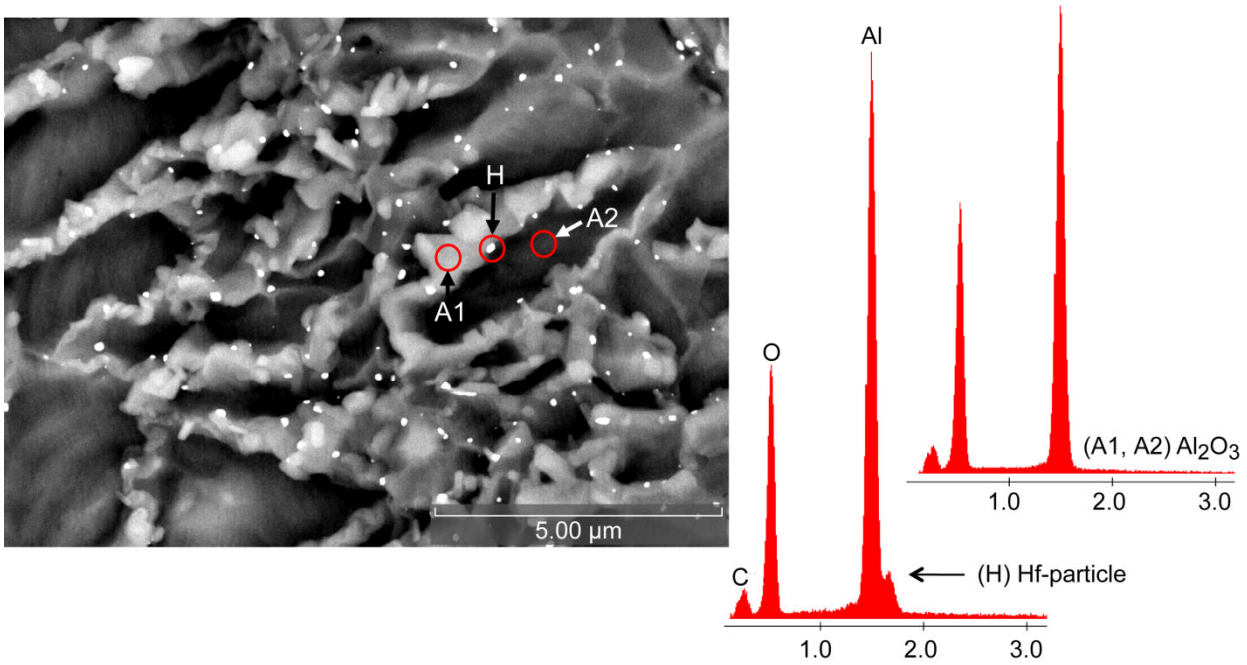

Figure 7.—BSE image centered on type I dense oxide ridge network and associated EDS spectra. Hf enrichment is shown at the fine bright particles (H) compared to pure Al_2O_3 at the clear regions of ridges (A1) or grain centers (A2) at, (15 kV).

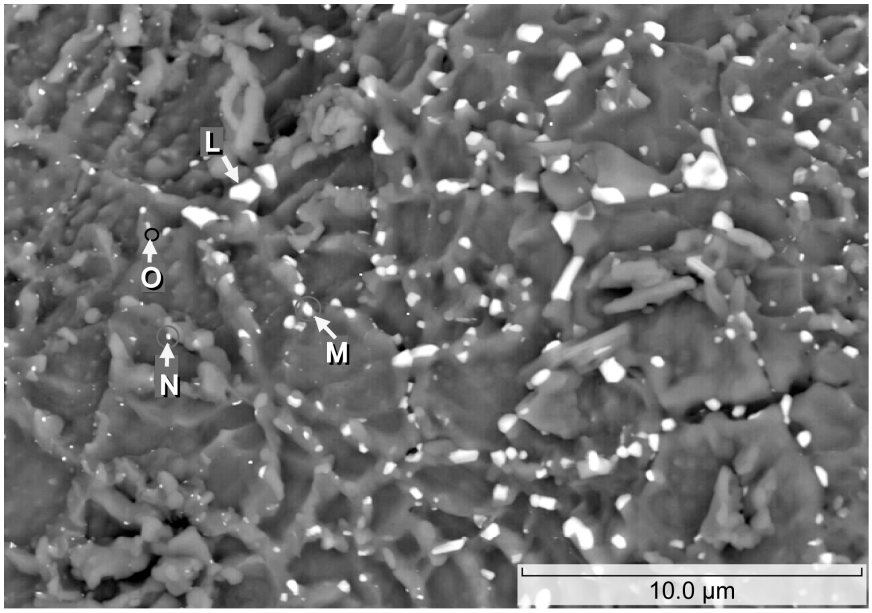

Figure 8.—BSE image of another region of type I oxides with a range of bright grain boundary particles, where particle L > M > N. A clean ridge, with no particle, is marked as point O, (15 kV).

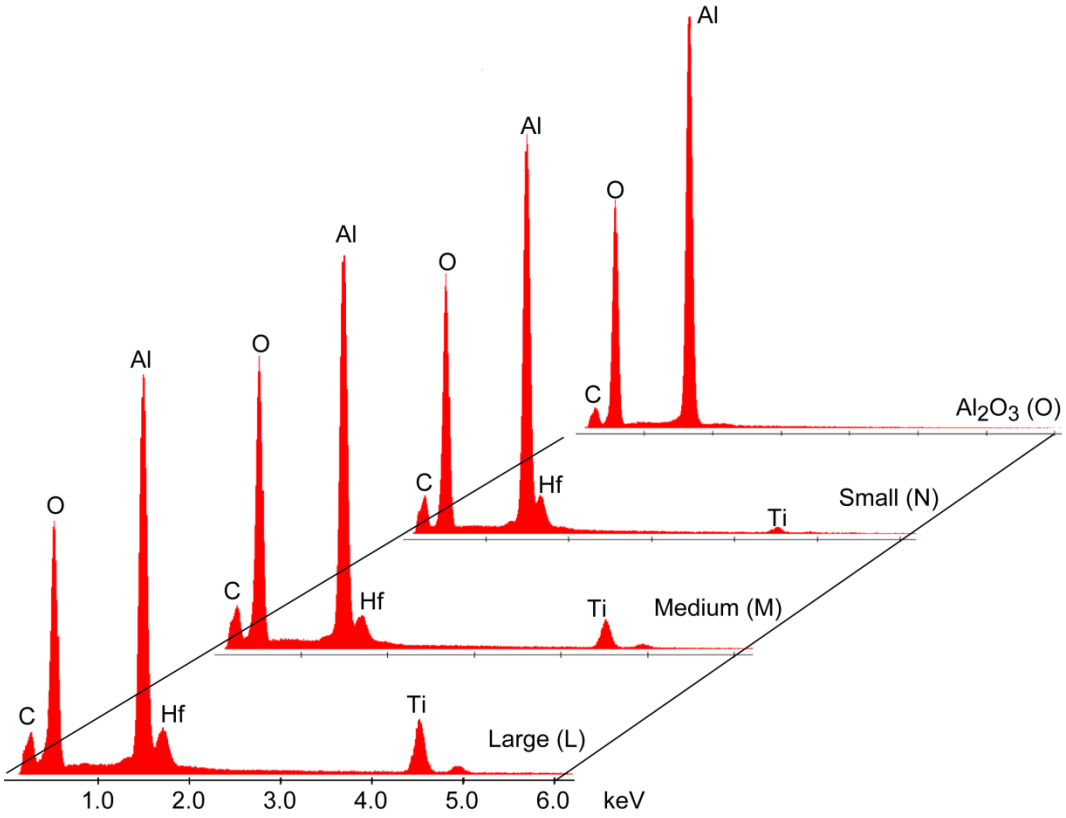

Figure 9.—EDS spectra of particles in Figure 8, where the peak intensity for Ti (L) > Ti (M) > Ti (N), at constant Hf; and no Hf or Ti at point O, (15 kV).

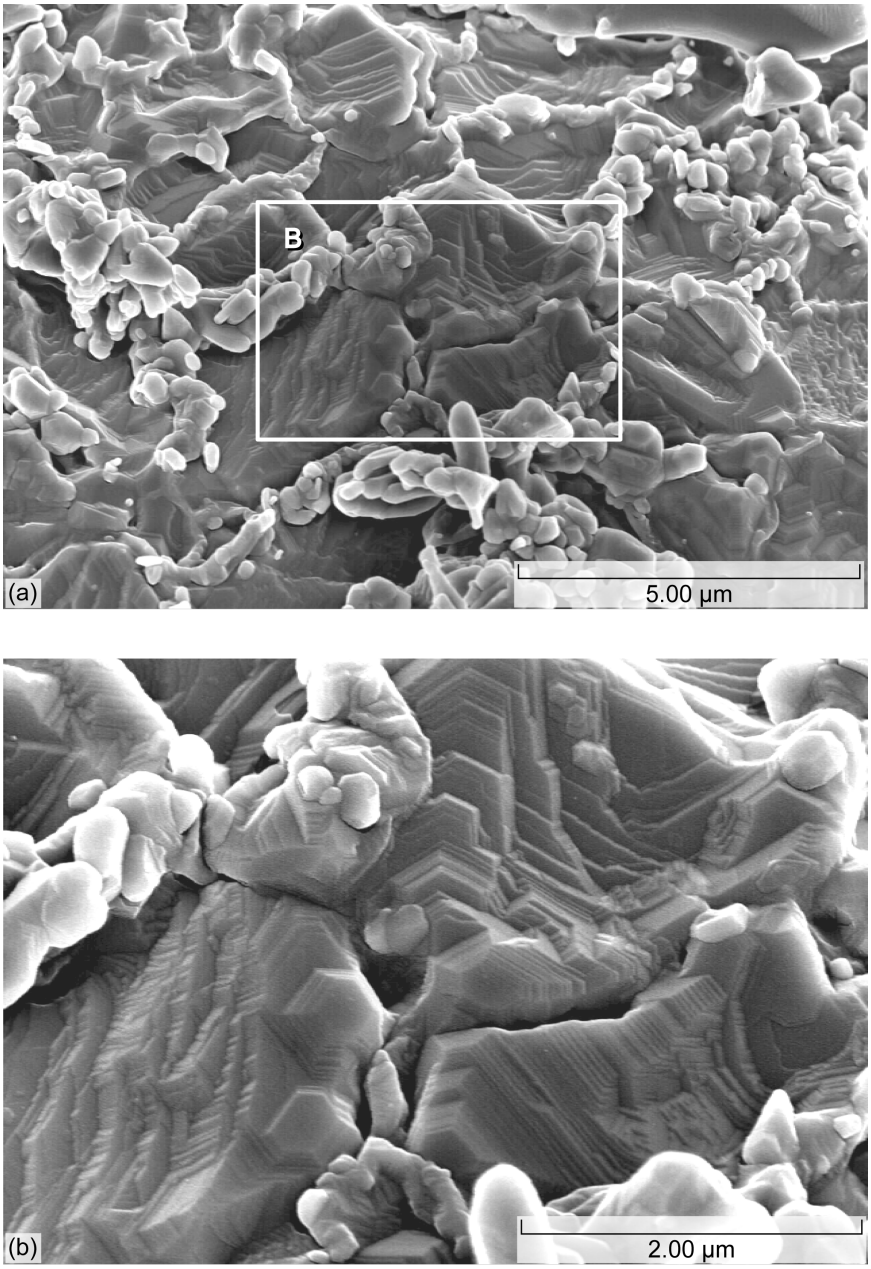

Figure 10.—Another region of type I oxide, (6 kV). (a) Grain boundary crystallites and center platelets, marked in frame B, selected for high-resolution imaging in (b). (b) Fine, crystallographically aligned steps and terraces.

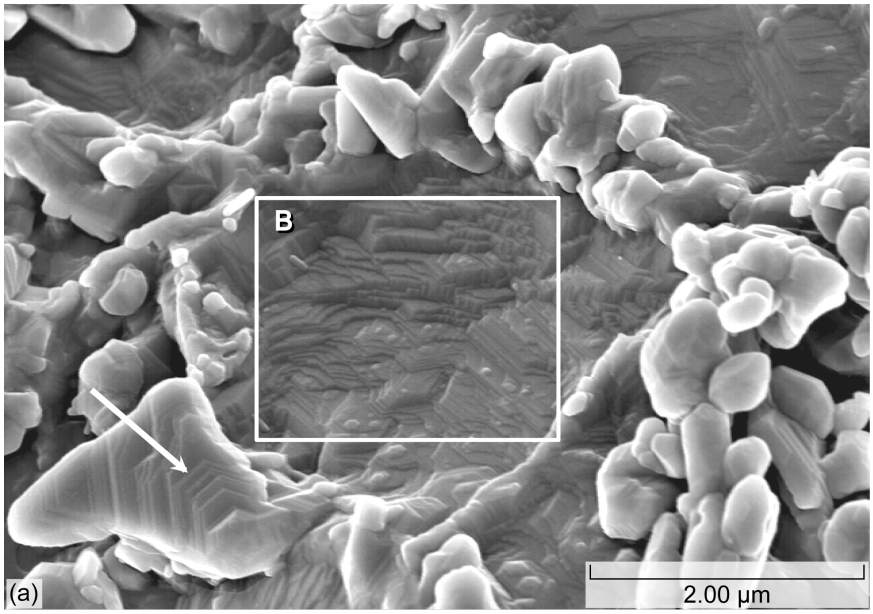

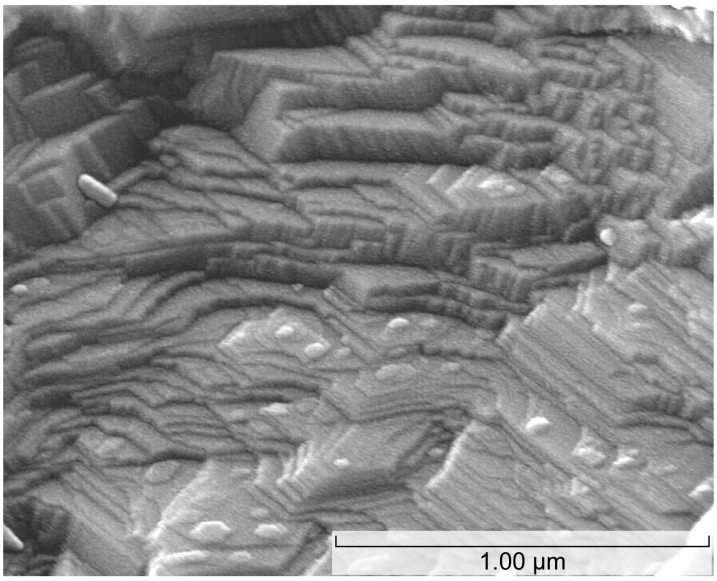

Figure 11.—Another high-resolution image of type I web structures, (6 kV).
(a) Crystallographically aligned striations in the boundary nodule (arrow).
(b) Central area, marked as frame B in (a), selected for displaying a complex arrangement of fine, crystallographically aligned steps and terraces.

Sample 1150–2 SEM

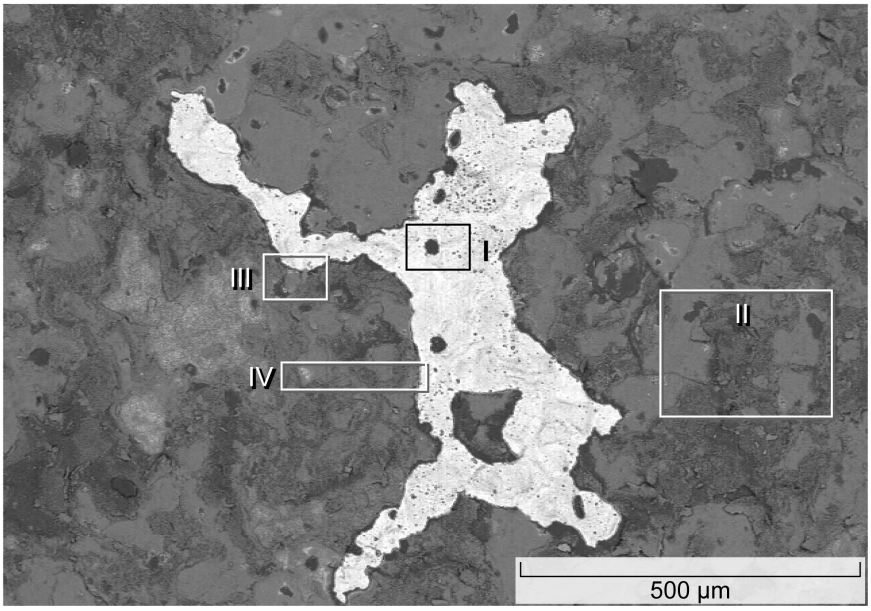

Figure 12.—BSE overview of Regions I through IV studied for less protective sample 1150–2 after 2000 1-h oxidation cycles at 1150 °C. Intensity variations indicate atomic weight variations and multiple scale types, (15 kV).

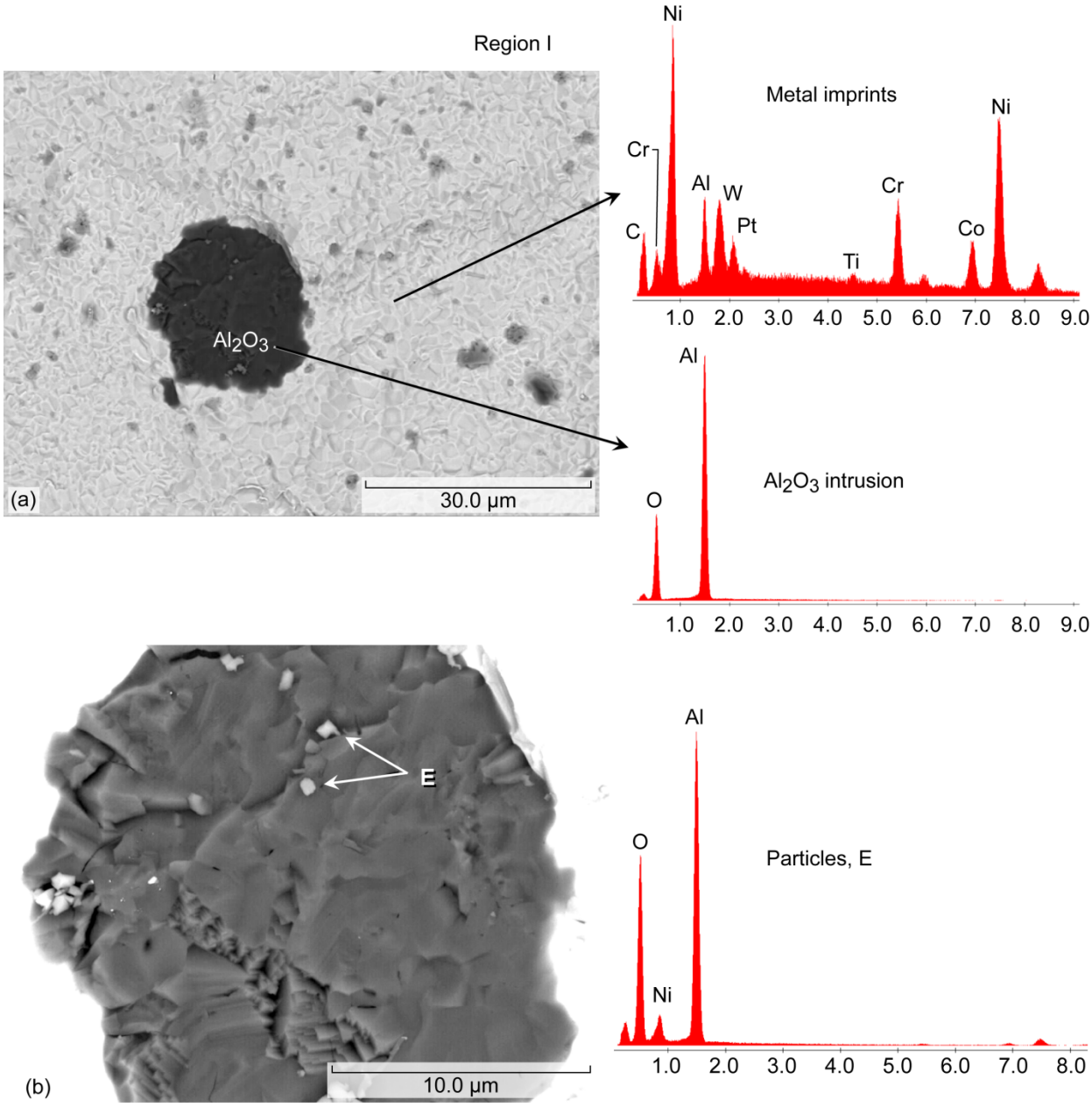

Figure 13.—An Al_2O_3 peg-like intrusion retained in region I of spalling to bare metal, (15 kV). (a) BSE/EDS spectra of pure Al_2O_3 island and surrounding metal. (b) BSE/EDS spectra indicating fine, Ni-rich inclusions in pure Al_2O_3 intrusion.

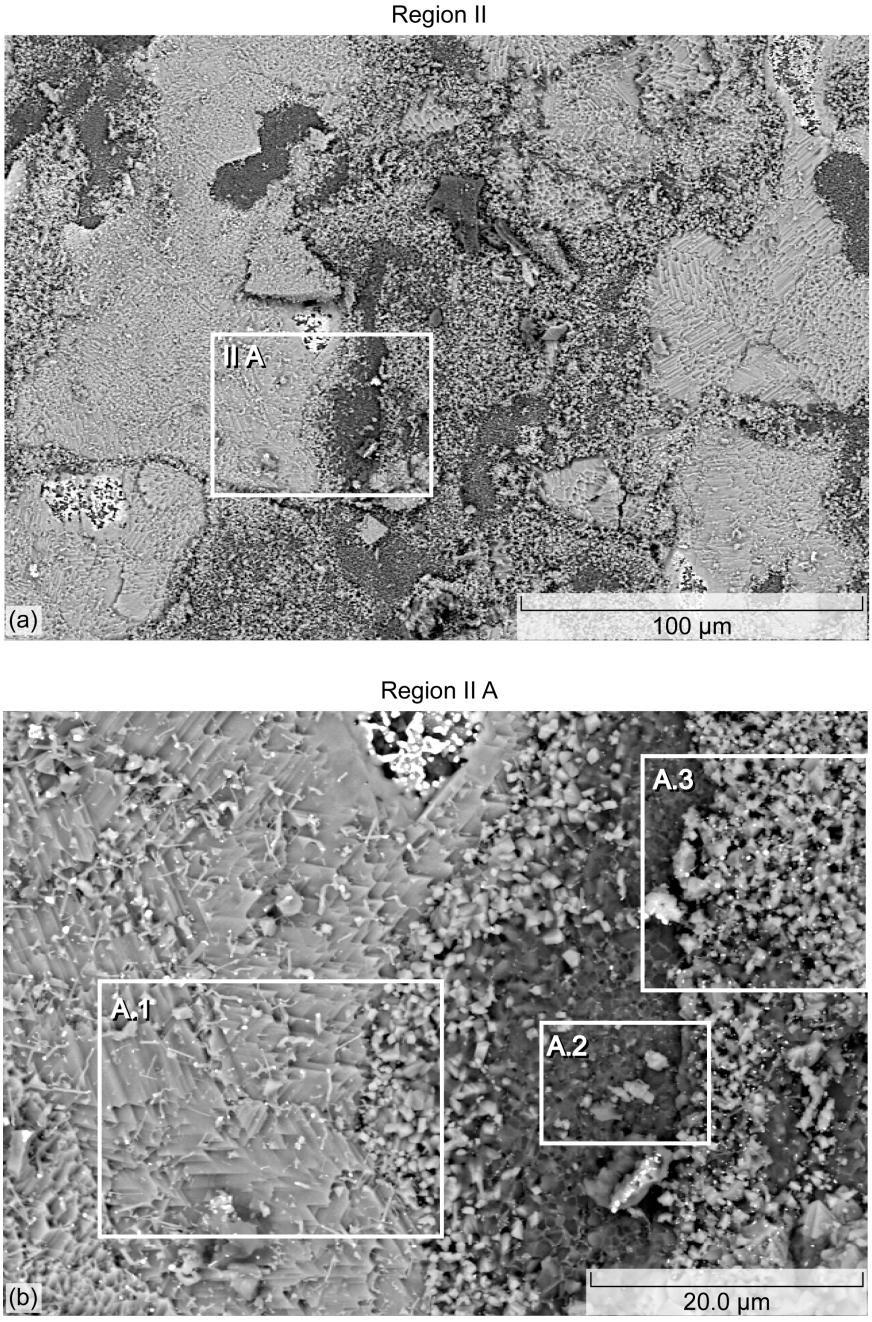

Figure 14.—BSE overview(s) of complex mosaic of various scale structures, (15 kV). (a) Repeated frequently within Region II overall. (b) Showing select, differentiated portions within Regions II, frames A.1, A.2, and A.3.

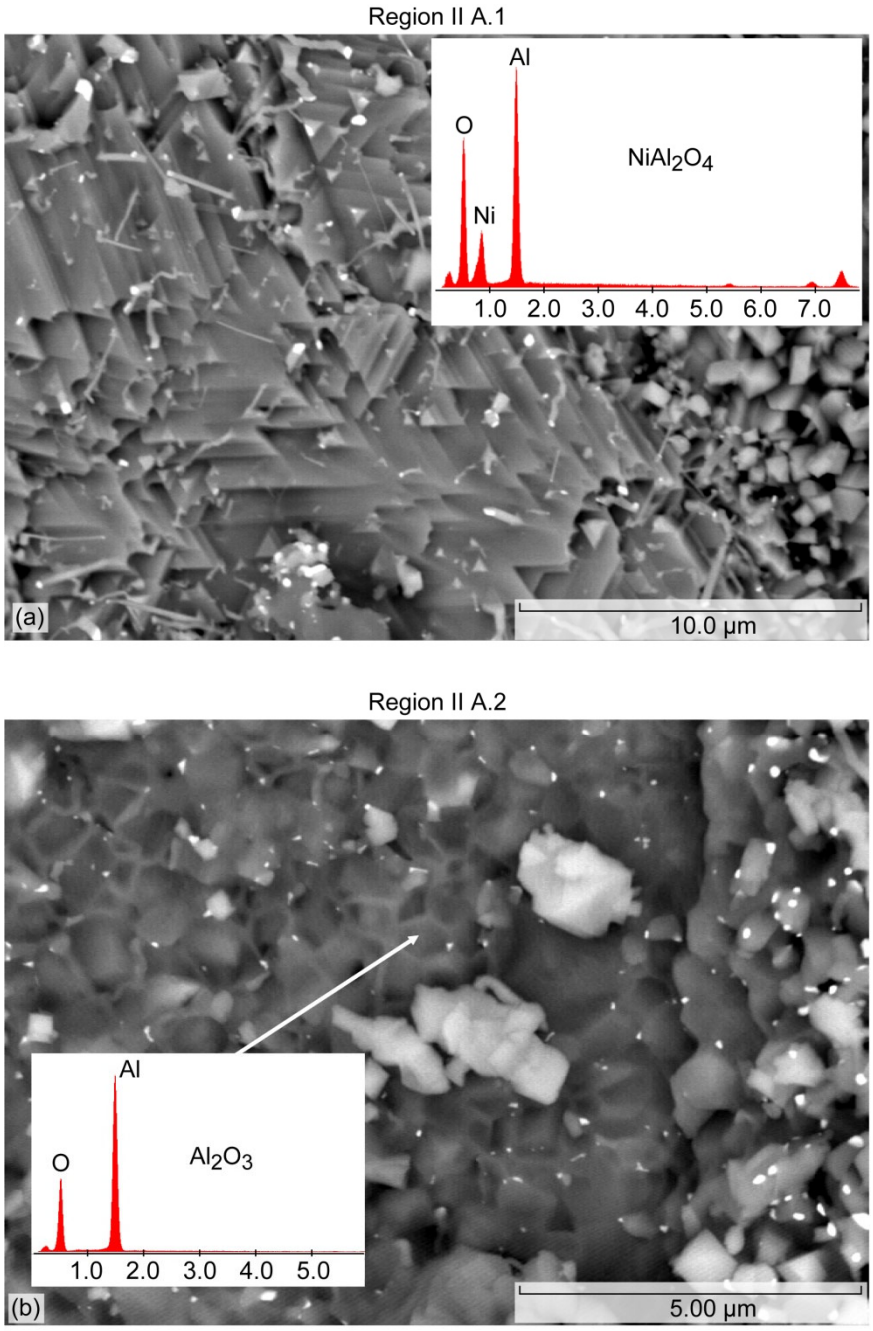

Figure 15.—Primary characteristics of Region II A (BSE/EDS at 15 kV). (a) Bright, crystallographically aligned, chevrons of an $NiAl_2O_4$ colony in Region II A.1 (b) Dark Al_2O_3 base layer in Region II A.2. (c) Fine, bright Ta,Ti-rich oxide particles B and D, grey $NiAl_2O_4$ grains, and dark Al_2O_3 base scale (C).

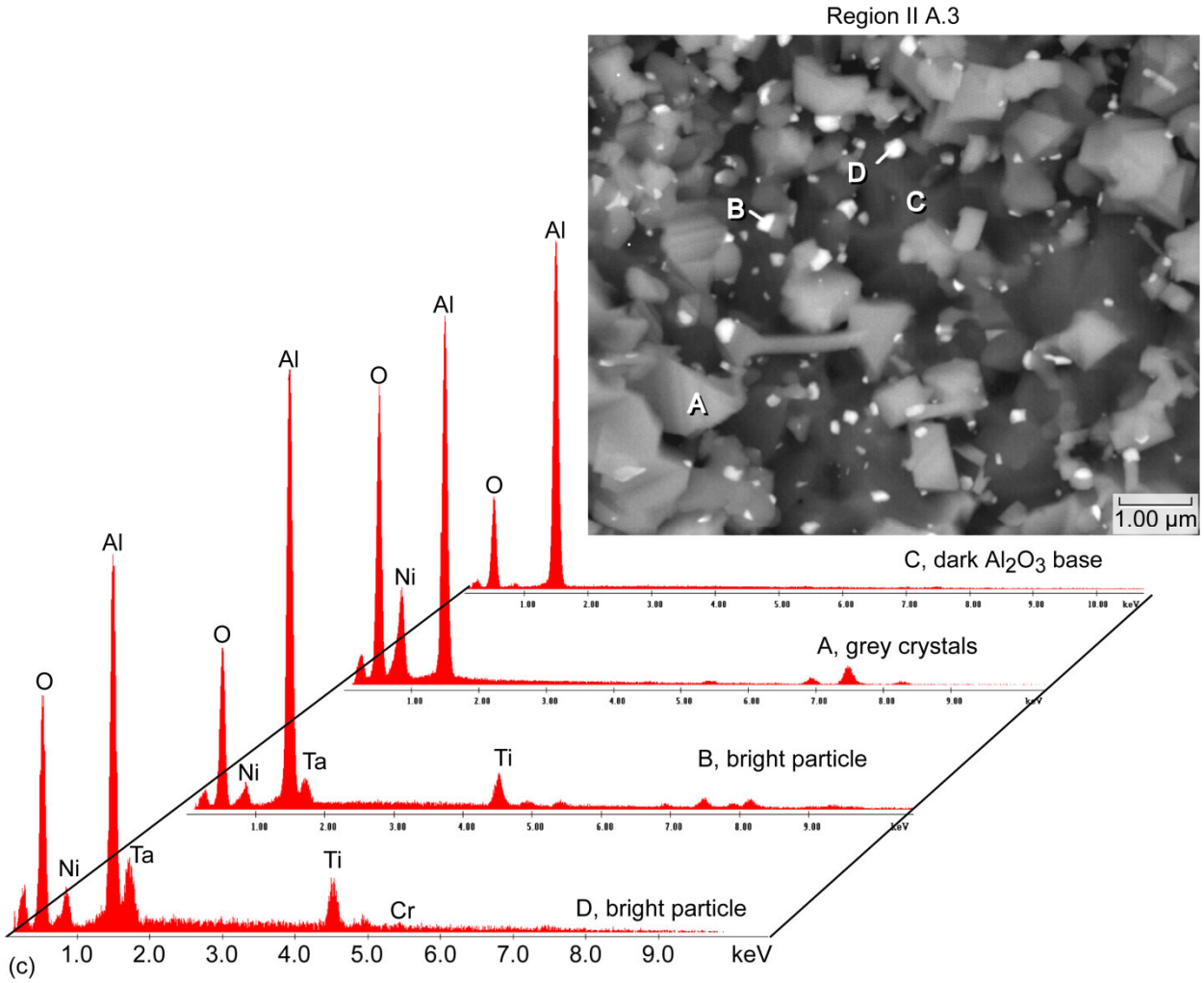

Figure 15.—Concluded. (c) Fine, bright Ta,Ti-rich oxide particles B and D, grey $NiAl_2O_4$ grains A, and dark Al_2O_3 base scale C.

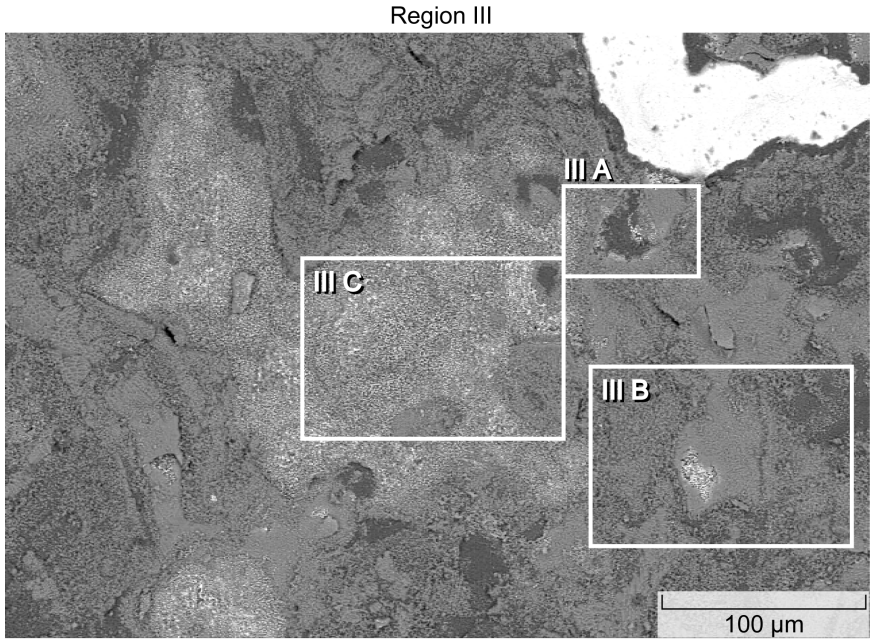

Figure 16.—BSE Overview of multiple structures found in Region III of Figure 12, (15 kV).

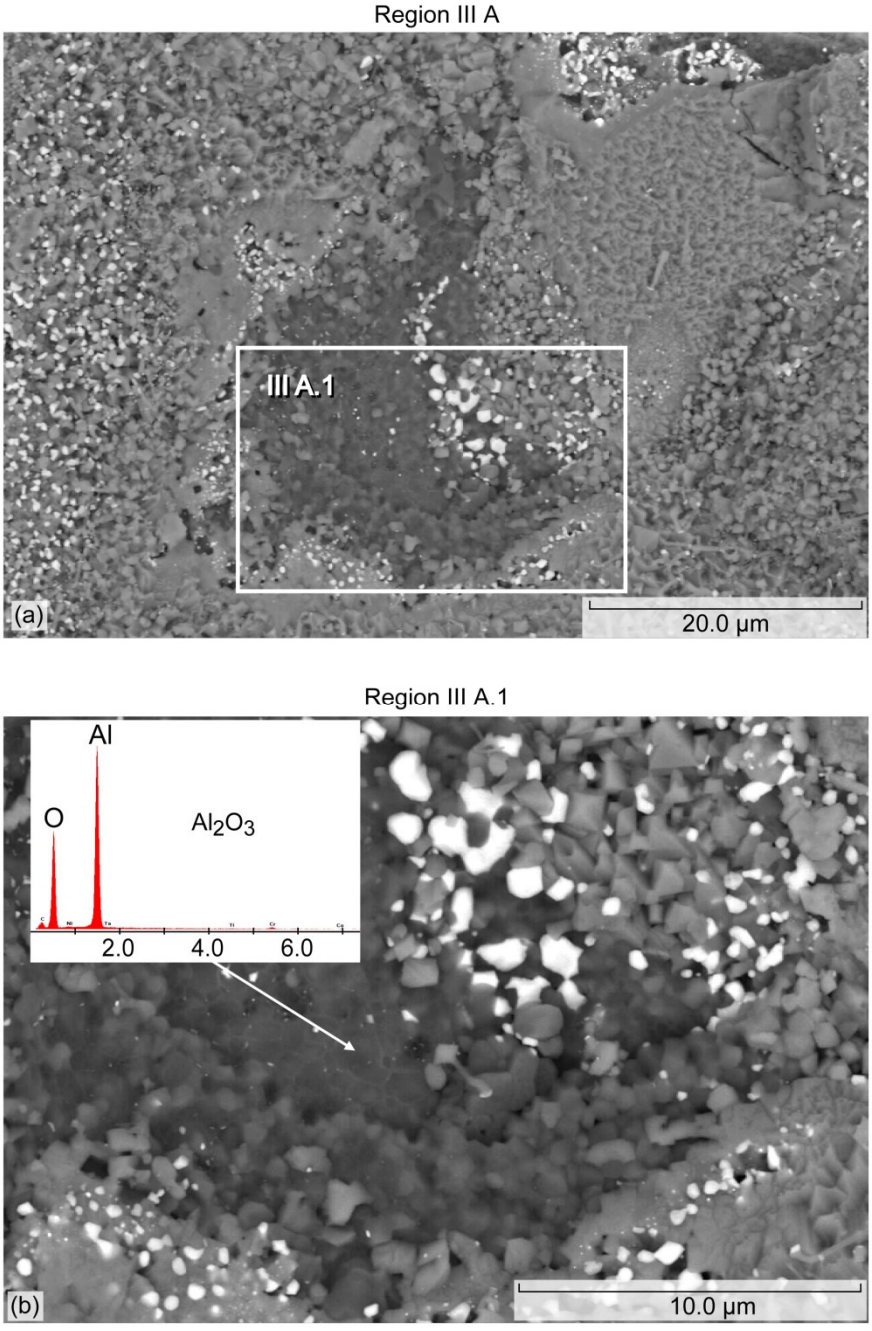

Figure 17.—Region III A of Figure 16 (BSE at 15 kV). (a) Gradation of bright, grey, and dark scale features. (b) Dark Al_2O_3 base layer from frame III A.1 in (a).

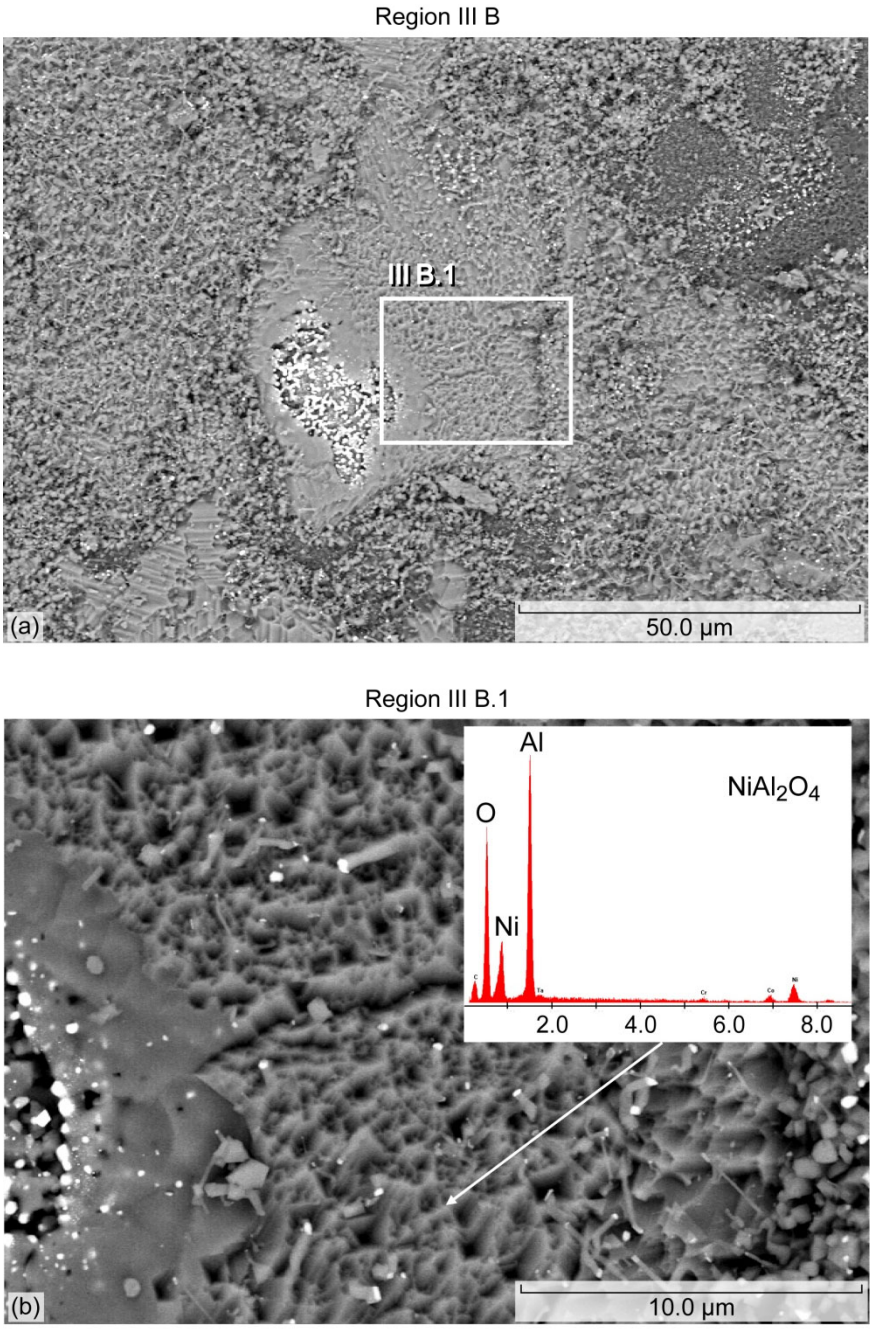

Figure 18.—Region III B of Figure 16 (BSE at 15 kV). (a) Preponderance of textured grey scale. (b) Detail of grey oxide from frame III B.1 in (a), showing faceted $NiAl_2O_4$ dimples.

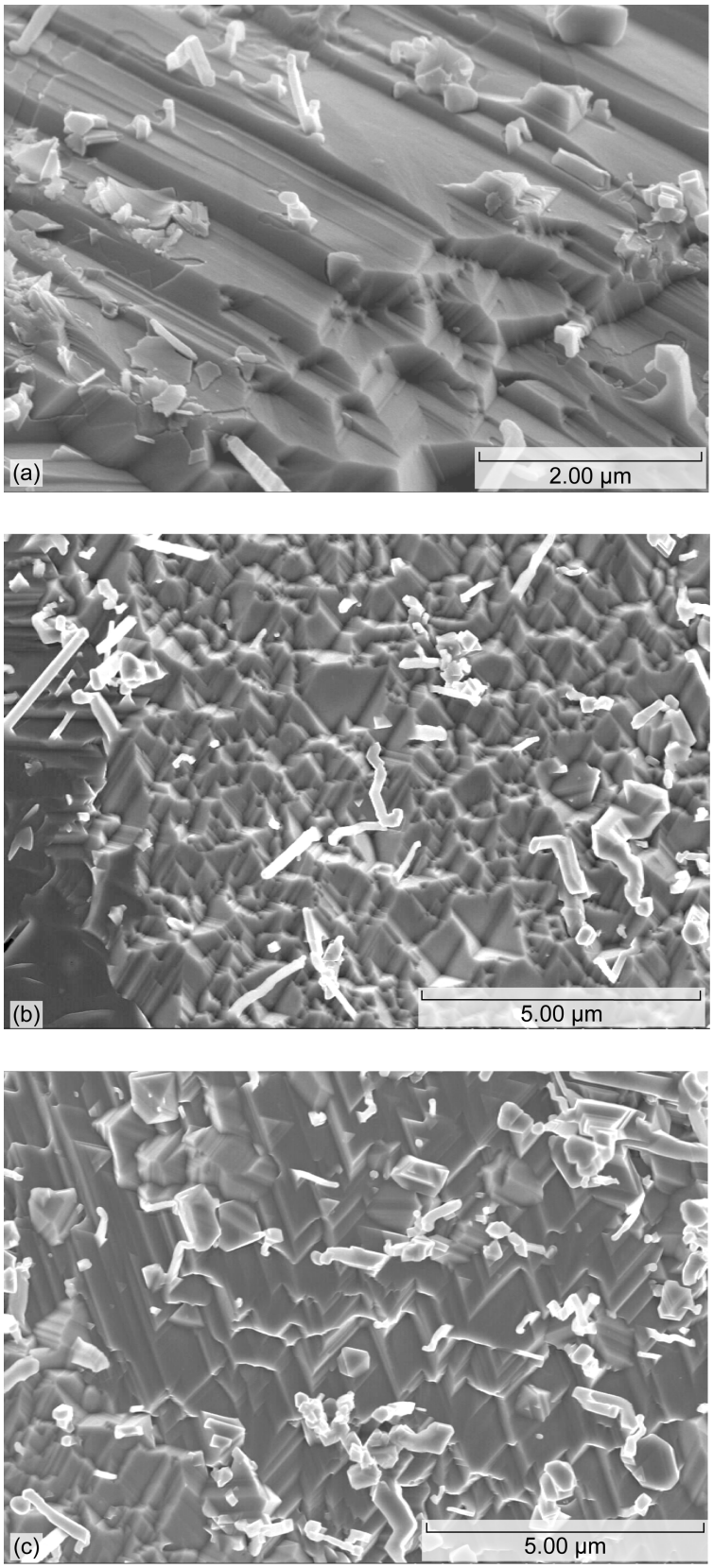

Figure 19.—Details of faceted dimples in various areas similar to Region III B.1 in Figure 18 (SE at 6 kV).

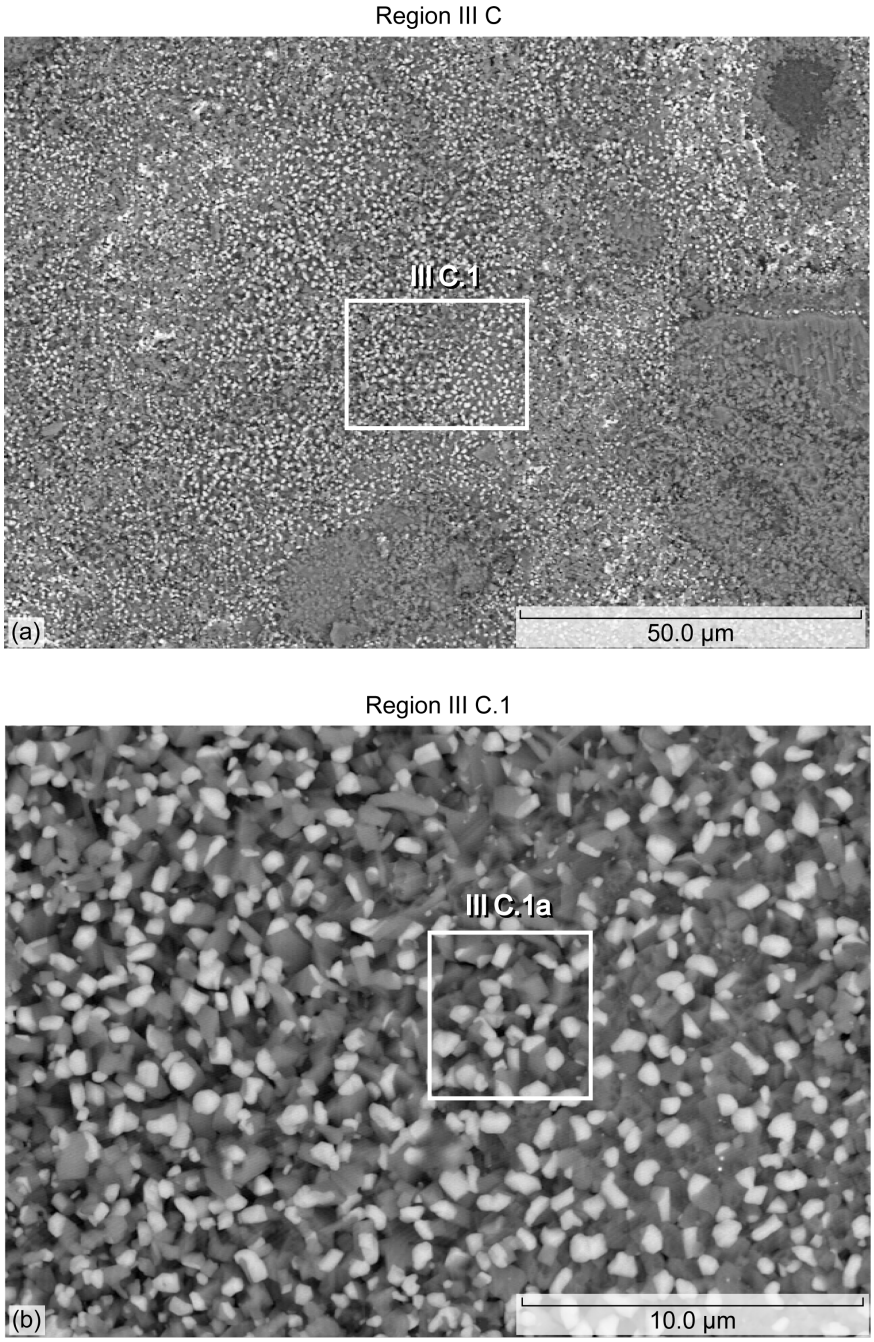

Figure 20.—Region III C structures (BSE/EDS at 15 kV). (a) Broad expanse of uniformly mottled scale in Region III C. (b) Equi-sized bright, grey, and dark nodular scale grains of Region III C.1. (c) Ta, Ti- rich white particles and $NiAl_2O_4$ grey grains make up the dominant scale features of Region III, frames C, C1, and C.1a marked in Figures 16 and 20(a) and (b).

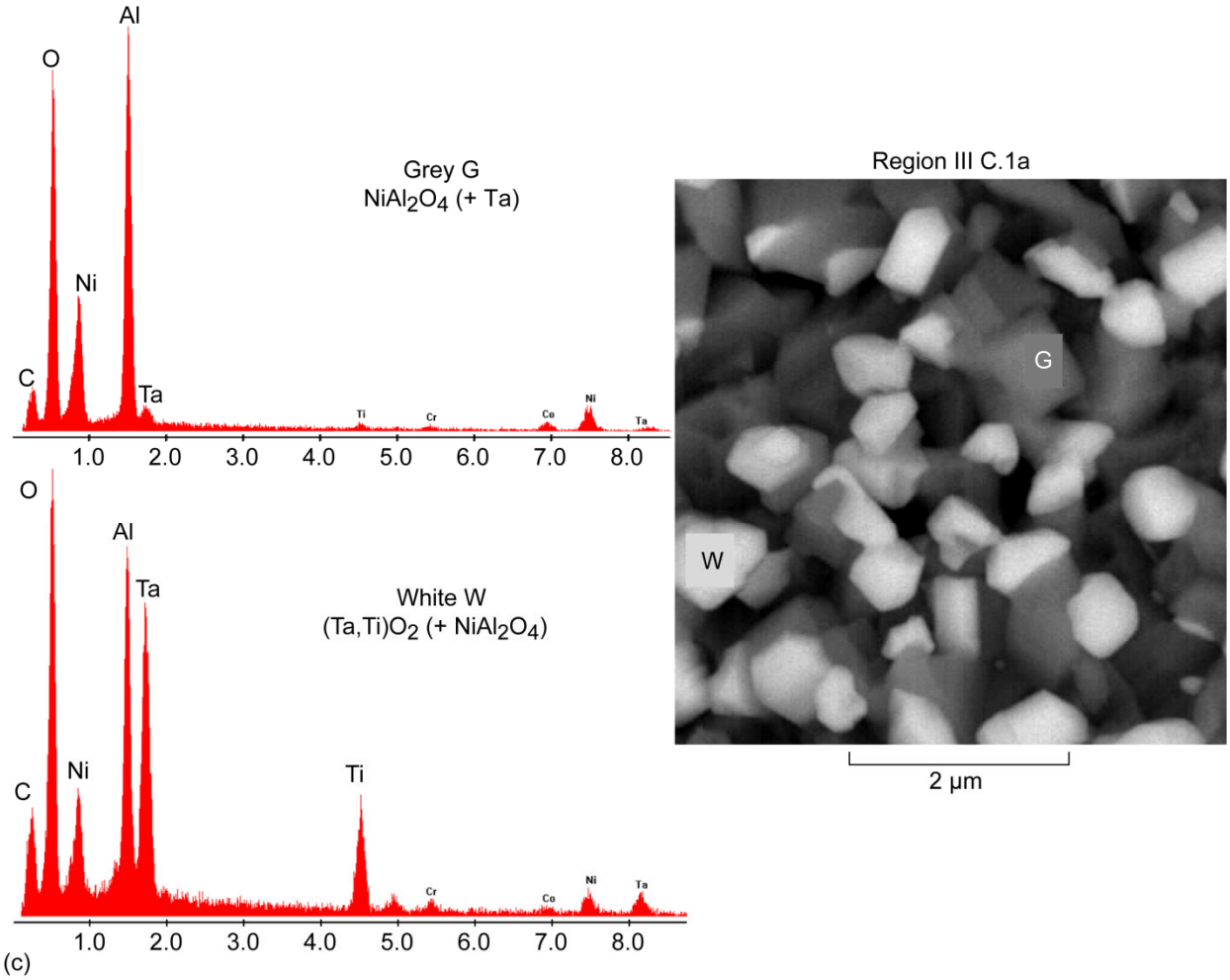

Figure 20.—Concluded. (c) Ta, Ti-rich white particles and $NiAl_2O_4$ grey grains make up the dominant scale features of Region III, frames C, C1, and C.1a marked in Figures 16 and 20 (a) and (b).

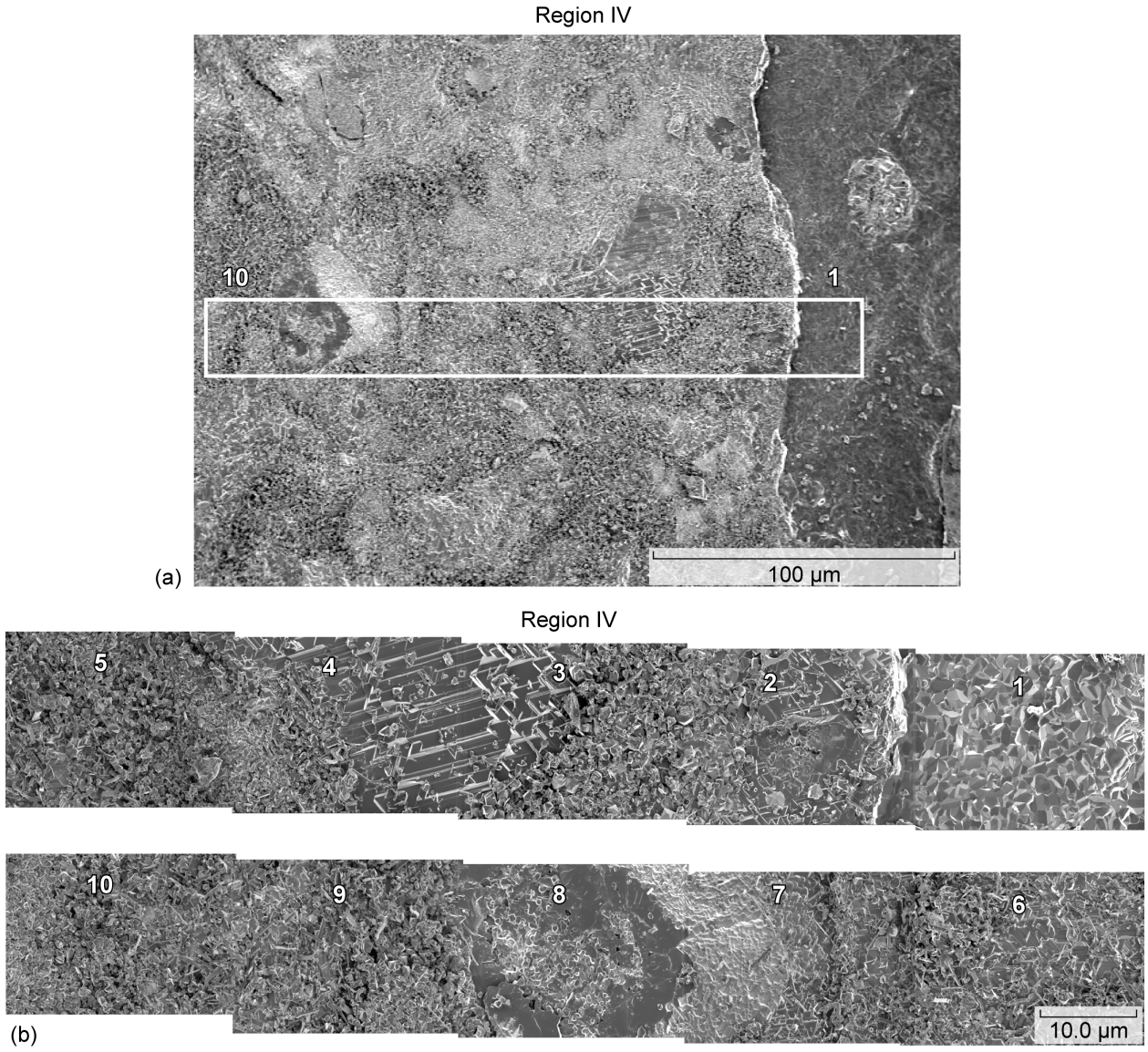

Figure 21.—Overview of Region IV marked in Figure 12 (SE at 1 kV). (a) Location of subsequent micrographs, numbered 1 to 10, right to left. (b) Contiguous montage of the 10 micrographs, in 2 strips.

Region IV–1

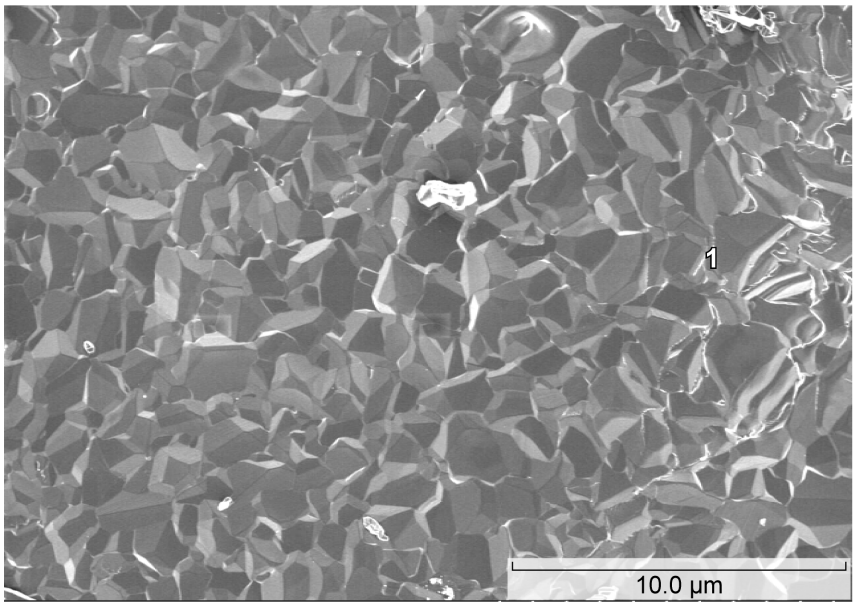

Figure 22.—Imprints of spalled alumina grains in metal, Region IV–1 from Figure 21(b), (1 kV).

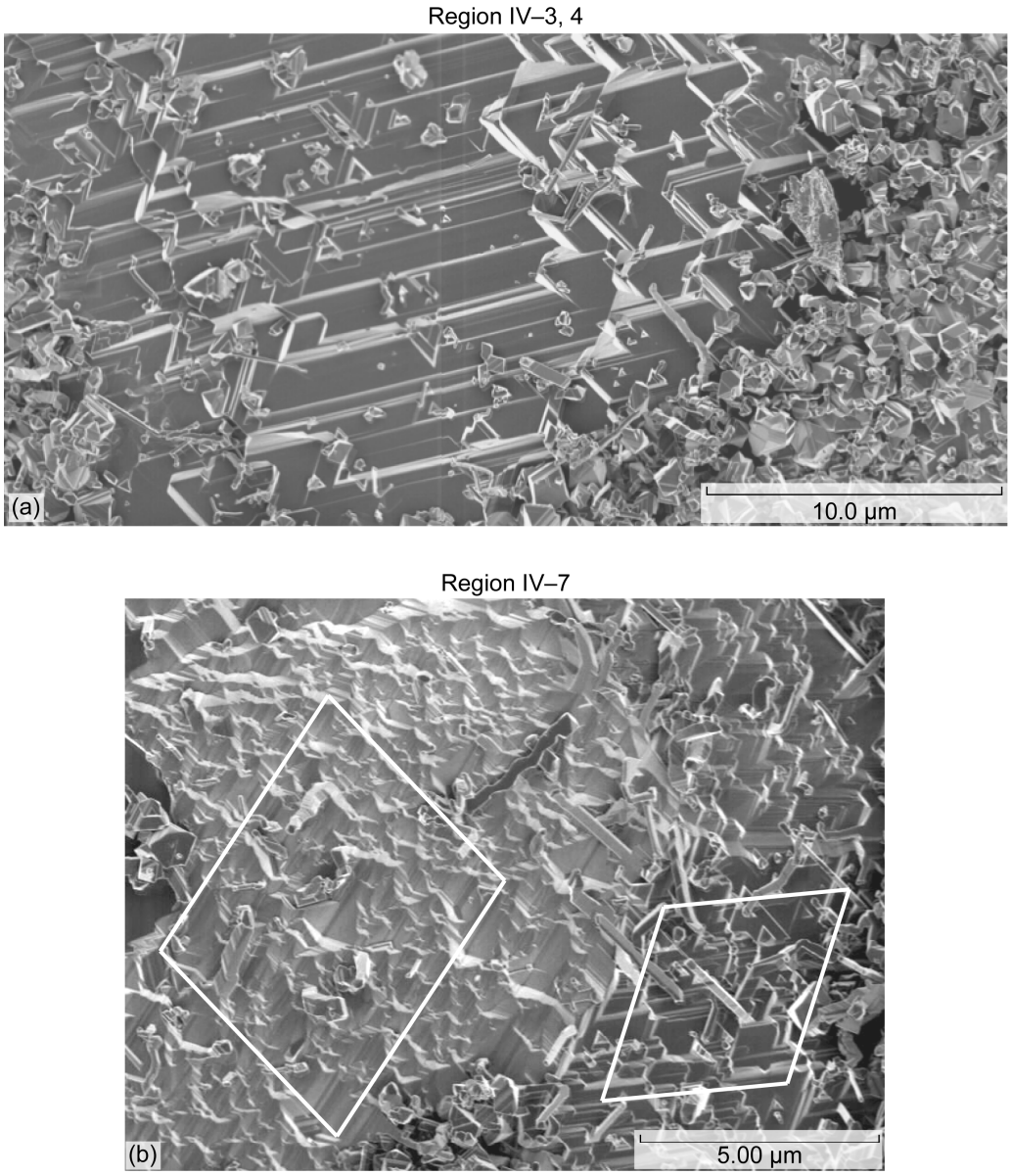

Figure 23.—Crystallographically faceted grains from frames marked in Figure 21(b), (1 kV). (a) Large aligned structure in region of frames IV–3 and 4. (b) Other oriented regions in frame IV–7. (c) Individually faceted nodular grains in frame IV–10.

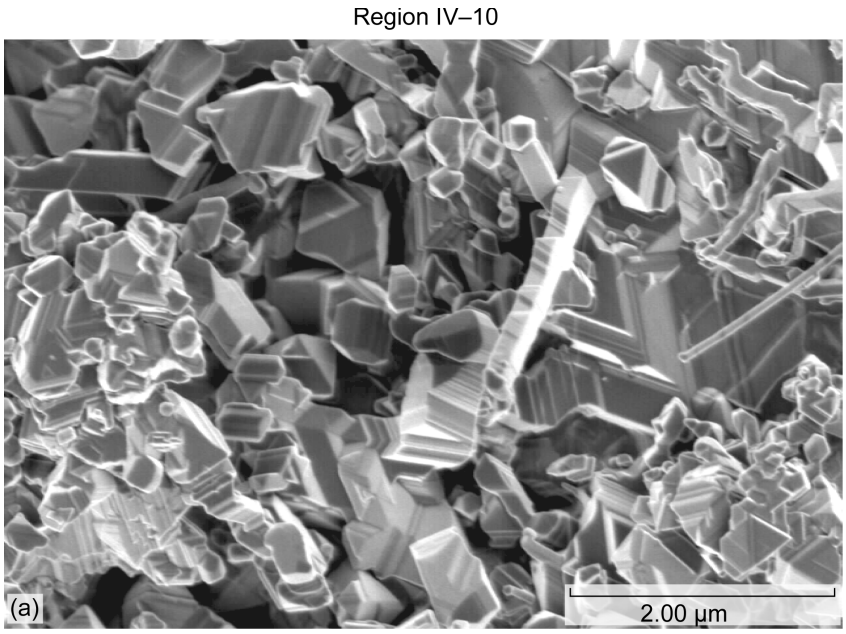

Figure 23.—Concluded. (c) Individually faceted nodular grains in frame IV–10.

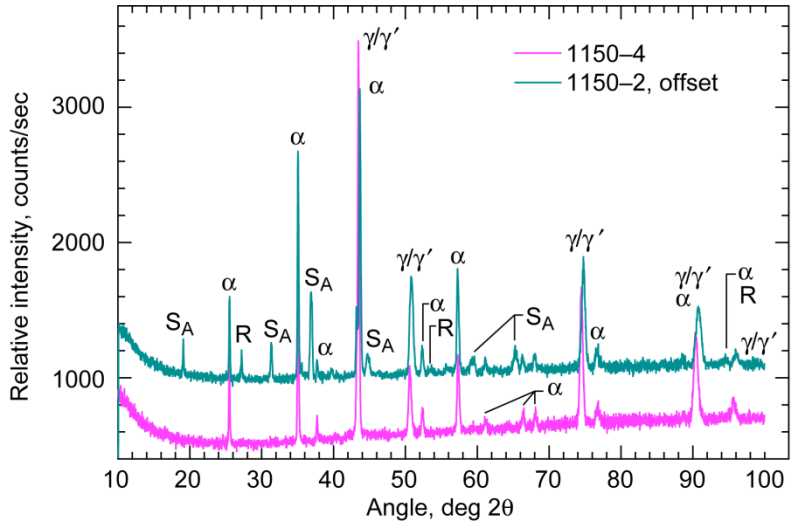

Figure 24.—Comparative X-ray diffractometer scans after 2000 1-h cycles at 1150 °C. Sample 1150–2 reveals strong α-Al_2O_3 (α), medium $NiAl_2O_4$ spinel (S_A), and weak rutile (R) oxide scale patterns. Sample 1150–4 exhibits exclusively α-Al_2O_3 (α). Both samples present strong patterns for the underlying and/or exposed γ/γ′-Ni/Ni_3Al metallic phase.

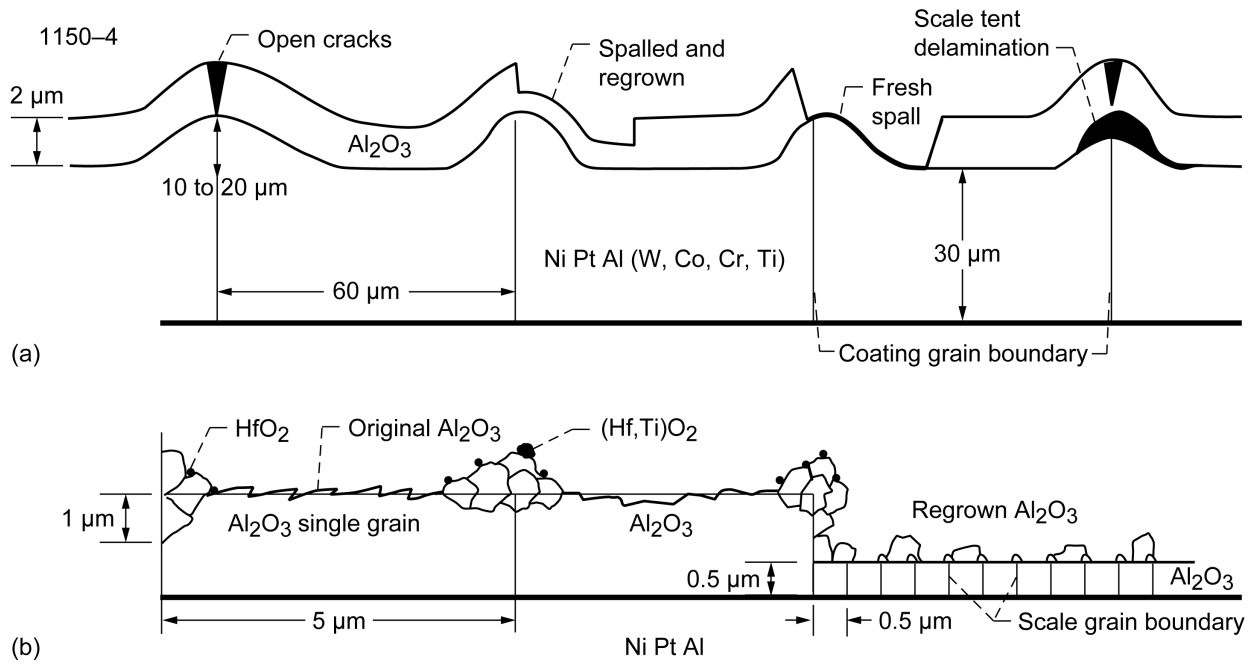

Figure 25.—Proposed schematic cross-section of surface region of sample 1150–4 after 2000 1-h cycles at 1150 °C. (a) Coating ridges at grain boundaries serve as scale failure sites (cracks and spalling). (b) Expanded view of scale showing "single crystal" α-Al_2O_3 spherulite platelets, polycrystalline region growing over prior α-Al_2O_3 spherulite boundaries, and fine (Hf,Ti)-rich oxide particles here. Spalled regions with re-grown, fine grain, non-spherulitic α-Al_2O_3.

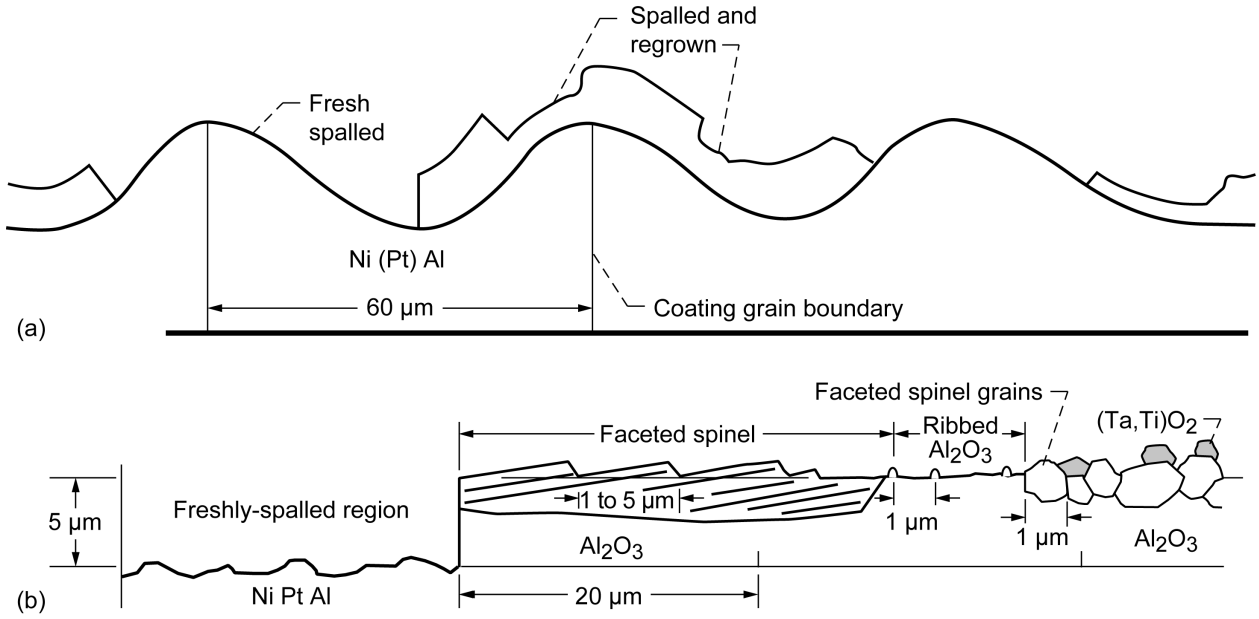

Figure 26.—Proposed schematic cross section of surface region of sample 1150–2 after 2000 1-h cycles at 1150 °C. (a) Coating ridges at grain boundaries served as prior scale failure sites, leading to widespread scale breakdown. (b) Expanded view of scale showing multiplex of surface morphologies and phases. Widespread, crystallographically faceted $NiAl_2O_4$ spinel or blocky spinel and (Ta,Ti)-rich oxide grains, all overlying a relatively featureless, fine grain α-Al_2O_3 base layer.

References

1. V.K. Tolpygo and D.R. Clarke, *Acta materialia*, 48 (2000) 3283–3293.
2. V.K. Tolpygo and D.R. Clarke, *Surface and Coatings Technology*, 203 (2009) 278–3285.
3. J.A. Haynes, B.A. Pint, K.L. More, Y. Zhang, and I.G. Wright, *Oxidation of Metals*, 58, (2002) 513–544.
4. P.Y. Hou and V.K. Tolpygo, *Surface and Coatings Technology*, 27 (2007) 623–627.
5. M.C. Maris-Sida, G.H. Meier, and F.S. Pettit, *Metallurgical Transactions*, 34A (2003), 2609–2619.
6. B.A. Pint, J.A. Haynes, Y. Zhang, K.L. More, and I.G. Wright, *Surface and Coatings Technology*, 201 (2006) 3852–3856.
7. Y. Zhang, J.A. Haynes, B.A. Pint, I.G. Wright, and W.Y. Lee, *Surface and Coatings Technology,* 163–164, (2003) 19–24.
8. M.W. Chen, M.L. Glynn, R.T. Ott, T.C. Hufnagel, and K.J. Hemker, *Acta materialia,* 51 (2003) 4279–4294.
9. J.L. Smialek, *Oxidation of Metals*, 72 (2009) 259–278 (also NASA/TM—2009-215664).
10. J.A. Nesbitt and J.L. Smialek, unpublished research, NASA Glenn Research Center, (2008).
11. B.A. Pint and K.L. More, *Journal of Materials Science*, 44 (2009) 1676–1686.
12. B.A. Pint, I.G. Wright, W.Y. Lee, Y., Zhang, K. Prüßner, and K. B. Alexander, *Materials Science and Engineering*, A245 (1998) 201–211.
13. V.K. Tolpygo, presented at the Science and Technology of Alumina Workshop, Schloss Ringberg, Germany (2002); also V.K. Tolpygo and D.R. Clarke, *Materials at High Temperature*, 20 (2003), 15–25.
14. D.W. Susnitzky and C. Barry Carter, *Journal of the American Ceramic Society*, 75 (1992) 2463–2478.
15. J.R. Heffelfinger, M.W. Bench, and C.B. Carter, *Surface Science*, 370 (1997) L168–L172.
16. L. Pham Van, O. Kurnosikov, and J. Cousty, *Surface Science*, 411 (1998) 263–271.
17. J.R. Heffelfinger, M.W. Bench, and C.B. Carter, *Surface Science,* 343 (1995) L1161–L1166.
18. A. Dent, S.B. Newcomb, and W.M. Stobbs, *Institute of Physics Conference Series*, 138, (1993) 429.
19. M.J. Li, X.F. Sun, H.R.Guan, X.X. Jiang, and Z.Q. Hu, *Oxidation of Metals*, 59 (2003) 483–502.
20. B. Bouchard, J. Balmain, F. Pedraza, *Oxidation of Metals*, 69, (2008) 193–210.
21. N. Vialas and D. Monceau, I, *Oxidation of Metals*, 66 (2006) 155–189: II, Oxid. Met., 68 (2007) 223–242.
22. H.M. Tawancy, A. Ul-Hamid, N.M. Abbas, M.O. Aboelfotoh, *Journal of Materials Science*, 43 (2008) 2978–2989.
23. Irene Spitsberg and Karren More, *Materials Science and Engineering*, A 417 (2006) 322–333.
24. M.W. Brumm, H.J. Grabke, *Corrosion Science*, 33 (1992) 1677–1690.

REPORT DOCUMENTATION PAGE	Form Approved OMB No. 0704-0188

1. REPORT DATE *(DD-MM-YYYY)*	2. REPORT TYPE	3. DATES COVERED *(From - To)*
01-02-2010	Technical Memorandum	

4. TITLE AND SUBTITLE
A Compendium of Scale Surface Microstructures: Ni(Pt)Al Coatings Oxidized at 1150 °C for 2000 1-h Cycles

5a. CONTRACT NUMBER

5b. GRANT NUMBER

5c. PROGRAM ELEMENT NUMBER

6. AUTHOR(S)
Smialek, James, L.; Garg, Anita

5d. PROJECT NUMBER

5e. TASK NUMBER

5f. WORK UNIT NUMBER
WBS 984754.02.07.03.16.02

7. PERFORMING ORGANIZATION NAME(S) AND ADDRESS(ES)
National Aeronautics and Space Administration
John H. Glenn Research Center at Lewis Field
Cleveland, Ohio 44135-3191

8. PERFORMING ORGANIZATION REPORT NUMBER
E-17136

9. SPONSORING/MONITORING AGENCY NAME(S) AND ADDRESS(ES)
National Aeronautics and Space Administration
Washington, DC 20546-0001

10. SPONSORING/MONITOR'S ACRONYM(S)
NASA

11. SPONSORING/MONITORING REPORT NUMBER
NASA/TM-2010-216091

12. DISTRIBUTION/AVAILABILITY STATEMENT
Unclassified-Unlimited
Subject Category: 26
Available electronically at http://gltrs.grc.nasa.gov
This publication is available from the NASA Center for AeroSpace Information, 443-757-5802

13. SUPPLEMENTARY NOTES

14. ABSTRACT
The surface structure of scales formed on Ni(Pt)Al coatings was characterized by SEM/EDS/BSE in plan view. Two nominally identical {100} samples of aluminide coated CMSX4 single crystal were oxidized at 1150 °C for 2000 1-h cycles and were found to produce somewhat disparate behavior. One sample, with less propensity for coating grain boundary ridge deformation, presented primarily α-Al_2O_3 scale structures, with minimal weight loss and spallation. The original scale structure, still retained over most of the sample, consisted of the classic θ-α transformation-induced ridge network structure, with ~25 nm crystallographic steps and terraces indicative of surface rearrangement to low energy alumina planes. The scale grain boundary ridges were often decorated with a fine, uniform distribution of $(Hf,Ti)O_2$ particles. Another sample, producing steady state weight losses, exhibited much interfacial spallation and a complex assortment of different structures. Broad areas of interfacial spalling, crystallographically-faceted $(Ni,Co)(Al,Cr)_2O_4$ spinel, with an α-Al_2O_3 base scale, were the dominant features. Other regions exhibited nodular spinel grains, with fine or (Ta,Ti)-rich (rutile) particles decorating or interspersed with the spinel. While these features were consistent with a coating that presented more deformation at extruded grain boundaries, the root cause of the different behavior between the duplicate samples could not be conclusively identified.

15. SUBJECT TERMS
Oxidation; Nickel aluminide; Platinum alloys; Coatings; Heat resistant alloys; Aluminum oxide; Moisture; Hydrogen embrittlement; Spallation

16. SECURITY CLASSIFICATION OF:			17. LIMITATION OF ABSTRACT	18. NUMBER OF PAGES	19a. NAME OF RESPONSIBLE PERSON
a. REPORT	b. ABSTRACT	c. THIS PAGE			STI Help Desk (email:help@sti.nasa.gov)
U	U	U	UU	40	19b. TELEPHONE NUMBER *(include area code)* 443-757-5802